TABLE OF CONTENTS

ABSTRACT (i)

ACKNOWLEDGEMENTS (ii)

INTRODUCTION 1

CHAPTER I - The Extracted Beam of the McGill Cyclotron 4

1. Introduction 4

2. Effect of Magnet Current 4

3. The Extracting Channel 9

4. The Steering Magnet 12

CHAPTER II - Circuitry 20

CHAPTER III - Background 25

CHAPTER IV - Experimental Methods 28

CHAPTER V - Results 32

(a) Po^{205m}

1. Experiments 32

2. Analysis 39

(b) Po^{207m1}

1. Experiments 46

2. Analysis 55

(c) Po^{207m2}

1. Experiments 58

2. Analysis 63

CONCLUSIONS 69

BIBLIOGRAPHY 72

APPENDIX I - Circuits 74

APPENDIX II - Probability Paper 84

ABSTRACT

The extracted beam of the cyclotron was modified to give a higher intensity of 1.31×10^{-10} amps. It had an energy of 90.6 Mev with a full width at half maximum of 1.2 Mev.

This was used to investigate Bi^{209} (p, xn) Po^{210-xn} reactions which produced short-lived isomeric states in Po. Two new isomers were discovered in Po^{207} and a new γ-ray was discovered in the decay of a previously known isomer in Po^{205}. A search in the energy range from 90 - 10 Mev, and in the time range from 10^{-5} sec to 10^{-1} sec was made with no other decays observed.

The two isomers in Po^{207} were found to have respectively γ-rays of 260 Kev(E3) with a half-life of 2.5 sec and 310 Kev (M2) with a half-life of 47 μsec, the latter being followed by an 820 Kev (E2) γ-ray. The 644 μsec isomer in Po^{205} was examined and found to have a new γ-ray at 160 Kev. Analysis of the system led to the assignment of this decay scheme as 160 Kev (M2) followed by a 707 Kev (E2).

These decays were compared with the level systematics in lead and the two short half-lives assigned as being from the i 13/2 state in polonium.

ACKNOWLEDGEMENTS

The author wishes to express his great appreciation to Dr. W.M. Martin for numerous helpful suggestions and his encouragement in the completion of this work. Thanks are due to Dr. J.S. Foster for his support and for making available the laboratory with its ample facilities. Much appreciation is felt for the many helpful suggestions of Dr. R.E. Bell.

Mr. S. Doig and his staff in the machine shop were most helpful in the construction of equipment and with suggestions in design, as was Mr. K. Heinstein in the construction of the electronics. Many thanks are due Mr. R.H. Mills for the operation of the cyclotron and discussions relative to it.

INTRODUCTION

An isomeric state of a nucleus may be defined as a state with energy and spin such that its decay to lower states has a measurable life time. This definition allows the inclusion of states with half-lives as short as 10^{-14} sec and isomers with half-lives as long as five years have been discovered.

An examination of the relative abundance of isomers, as a function of half-life, shows that there is a gap in the millisecond region with few isomers in comparison with other regions. There are in the time range 10 μsec to 0.1 sec only twenty-eight isomers[1-28] recorded at present and most of those have been discovered in the last five years.

In a summary of nuclear isomerism, Goldhaber and Sunyar[9] state: "They (millisecond isomers) cannot be expected to be very common, and the fact that they have so far escaped detection need not be entirely due to experimental difficulties". This statement implies that the Weisskopf estimates suggest they are more unlikely than other half-lives. At the same time R.D. Evans [29] says: "Experimental techniques for the exploration of the millisecond domain await development and systematic utilization". These statements indicate the possibilities in an investigation in this region.

Perhaps one of the main difficulties in the study of this region has been the development of the techniques. Delayed coincidence measurements, which work well for half-lives shorter than 10 μsec, become difficult for longer determinations due to the high

chance coincidence rate which makes lengthy background corrections necessary [30]. The general method used here is best described as the "pulsed Accelerator Technique". It was first tried at this laboratory by W.T. Link[14] and has been continued by the present author. The nuclei to be studied are produced by bombarding an element in the 90 Mev external beam of the McGill Synchrocyclotron. The protons arrive in bursts which last for 40 μsec, with a period variable from 2.5 msec to 1 sec. The γ-rays from the target are detected between bursts by a NaI(Tl) crystal and analyzed with respect to time and energy.

Several changes have been made in the instrumentation and in the experimental environment with respect to Link's[14] work. A new time analyzer has been built. The current in the external beam has been increased and the background has been decreased by the construction of a new counting castle.

The present system allows the measurement of the following properties of nuclear isomerism:

1. The excitation function.

2. The isotopic assignment from critical absorber experiments on the X-rays.

3. The K-conversion coefficients in heavy elements and in certain cases the total conversion coefficients of the γ-rays involved.

4. Under best conditions, the multipolarity of the γ-rays and the spins and parities of the levels.

5. Half-lives between 2×10^{-5} sec and 10 sec.

With these changes two new isomers have been discovered in Po^{207} and additional information has been obtained on Po^{205} previously studied by Link[14].

In brief, the two new isomers found were Po^{207m_1} and Po^{207m_2}. Po^{207m_1} has a half-life of 47 ± 3 μsec. It is de-excited by emission of two γ-rays, one 315 Kev (M2), the other 820 Kev (E2). Po^{207m_2} has a half-life of 2.5 ± 1 sec. It de-excites by emission of one 260 Kev (E3) γ-ray to the isomeric state of Po^{207m_1}. The previously found isomer in Po^{205m} was re-examined and a new γ-ray was found of 160 Kev. It was assigned as an M2 and the other γ-ray of 707 Kev was assigned as E2.

CHAPTER I

THE EXTRACTED BEAM OF THE MC GILL CYCLOTRON

1. Introduction

The external beam system is shown in Fig. 1. The internal beam is scattered into a magnetic channel by a Uranium foil placed at a radius of 36" in the cyclotron. From the channel it is taken to the steering magnet by which it is bent and sent through the 11' wall into the corridor leading down to the cyclotron. The counting is done in the corridor. After the beam passes through the counting castle it goes into a sink. It was decided to study the beam system with a view to increasing the beam current without changing the general method.

2. Effect of Magnet Current

The first step in this study was a measurement of the external beam current at the exit port of the cyclotron. The measurement was made with a Faraday cup and studied as a function of the cyclotron magnet current, Fig. 2 curve I. The important feature of this curve is the sharp rise in the external beam current at a cyclotron magnet current of 640 amps. This rise is followed by a slight drop as the cyclotron magnet current is increased further.

To explain these phenomena a study was done on the internal beam. The internal beam current was plotted as a function of radius with the cyclotron magnet current held constant. This measurement was repeated for a series of magnet currents. The results are plotted in Fig. 3. It is noted that as the magnetic field is increased

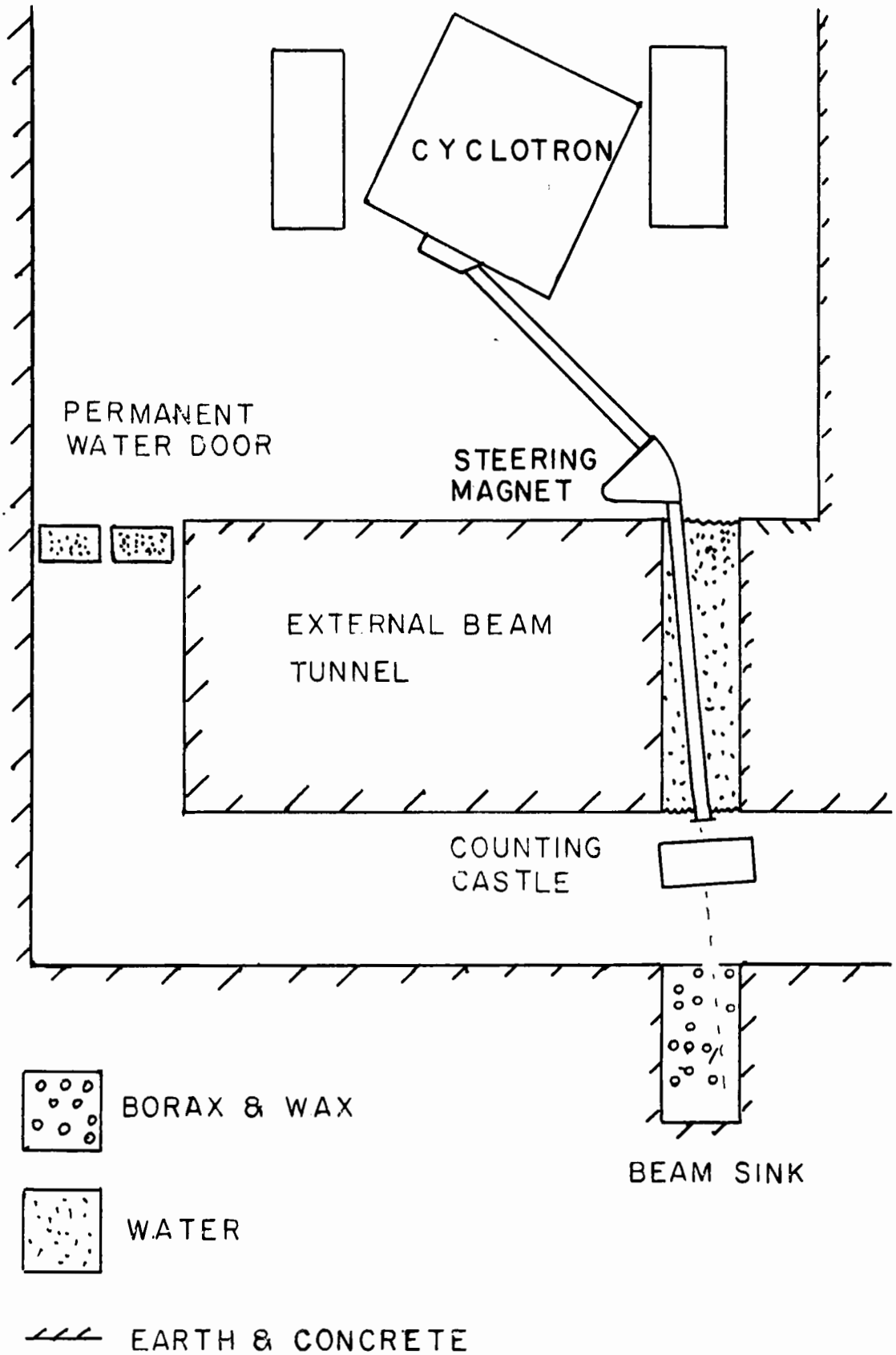

FIG. 1. PLAN VIEW OF CYCLOTRON & PROTON BEAM

FIG. 2

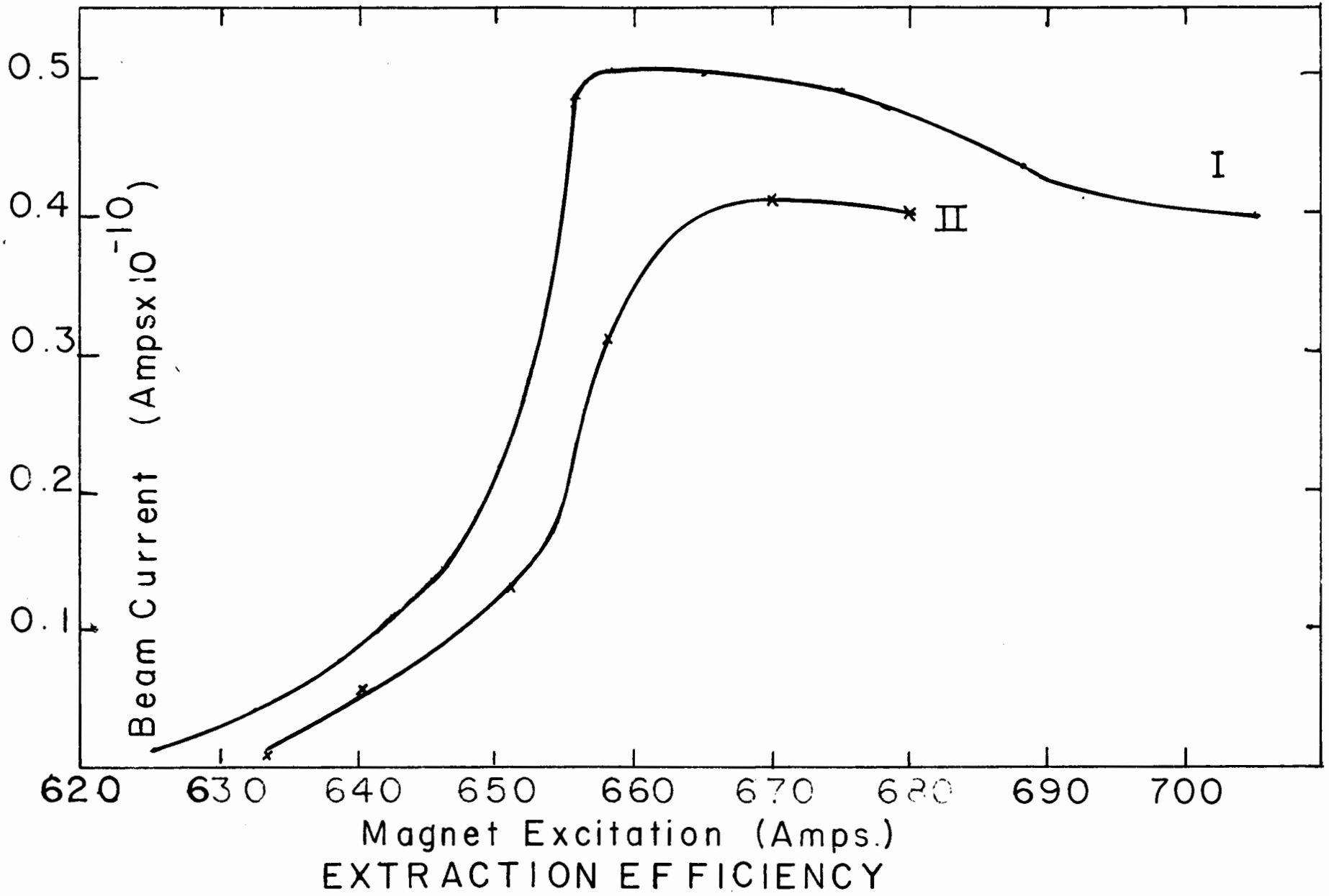

EXTRACTION EFFICIENCY

FIG. 3

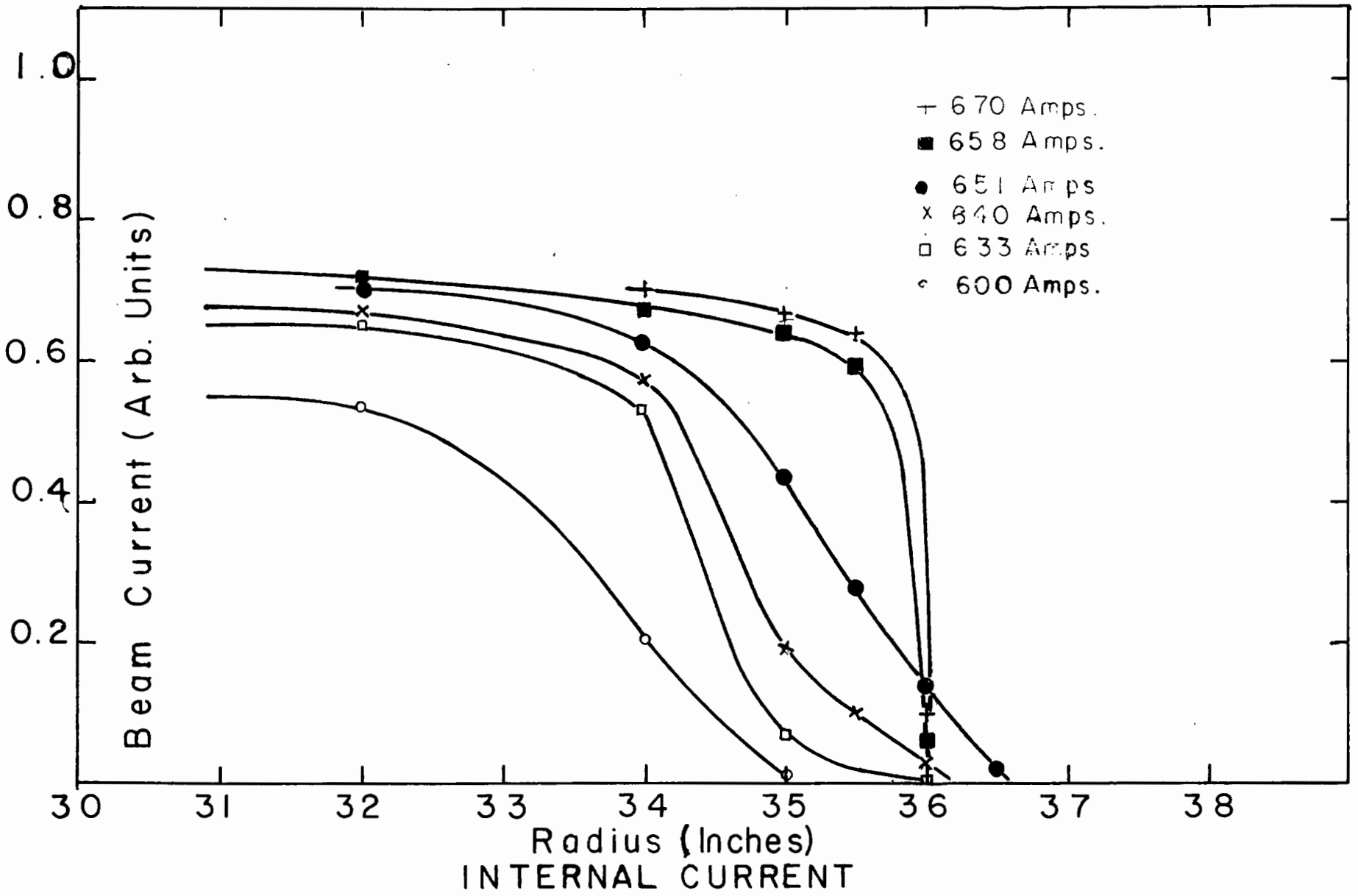
1.0
0.8
0.6
0.4
0.2
Beam Current (Arb. Units)
+ 670 Amps.
■ 658 Amps.
● 651 Amps
x 640 Amps.
□ 633 Amps
◦ 600 Amps.
30
31
32
33
34
35
36
37
38
Radius (Inches)
INTERNAL CURRENT

the internal beam reaches a greater radius. From the curves of Fig. 3 the beam currents for a radius of 35.75" were read and then were replotted as a function of cyclotron magnet current in Fig. 2, curve II. This is effectively a measurement of the current hitting the scatterer as a function of cyclotron magnet current, and the similarity of this curve with curve I of the same figure shows that the increase in the external beam was due to more beam reaching the scatterer.

The internal current (curve II) is the same at 680 amps as at 660 amps, but the external current has dropped somewhat (curve I). Since the higher current means stronger field and smaller radius of curvature the protons accepted by the exit channel will be those which were scattered at a larger angle. Coulomb scattering drops rapidly with angle and hence the fraction of protons striking the scatterer and accepted by the exit channel is reduced by increasing the magnet current. The extracted beam as a function of magnet current should therefore exhibit a maximum, and this maximum occurs at approximately 660 amps.

The cyclotron is normally operated at a current of 620 amps. To avoid placing a considerably increased load on the magnet cooling system, an attempt was made to bring the internal beam all the way out to the scattering foil at the lower magnet current.

The cyclotron coils are wound with extruded aluminum ribbon and the cooling water flows through the extrusion. The aluminum is wrapped around the magnet in two coils of eight layers each with the cooling water flowing in at the centre and out at the

ends of each layer. Each of these layers for the lower coil is designated as in Fig. 5.

The distribution of ampere-turns can be altered by shunting or short-circuiting any one of these half-layers. The cyclotron is normally run with 8i shorted out. Characteristic curves of current versus radius were taken with various half-layers of the lower coil shorted out in turn. These curves are shown in Fig. 4 where the cyclotron was run at 620 amps. The only significant improvement was shown in the case 2o, but this was not enough to warrant any changes. Similar sets of curves were taken for 640 and 660 amps without any major effects. Consequently, cyclotron is run at 660 amps with 8i shorted out.

3. The Extracting Channel

The fringing field of the cyclotron and the flux in the extracting channel were changed by the increased operating current of the cyclotron. This meant that the focussing of the external beam on the steering magnet was changed. The beam at the steering magnet was diverging and about 5" in diameter. The centre of the beam was $\frac{1}{2}$" high and 2" to the right with respect to the entrance aperture of the steering magnet.

It was necessary to improve the focussing and to adjust the direction of the extracted beam before it enters the steering magnet. There is a gap in the exit channel through which the standard target probe passes. One can mount a pair of wedges on this probe and so place the wedges in the gap that the protons pass

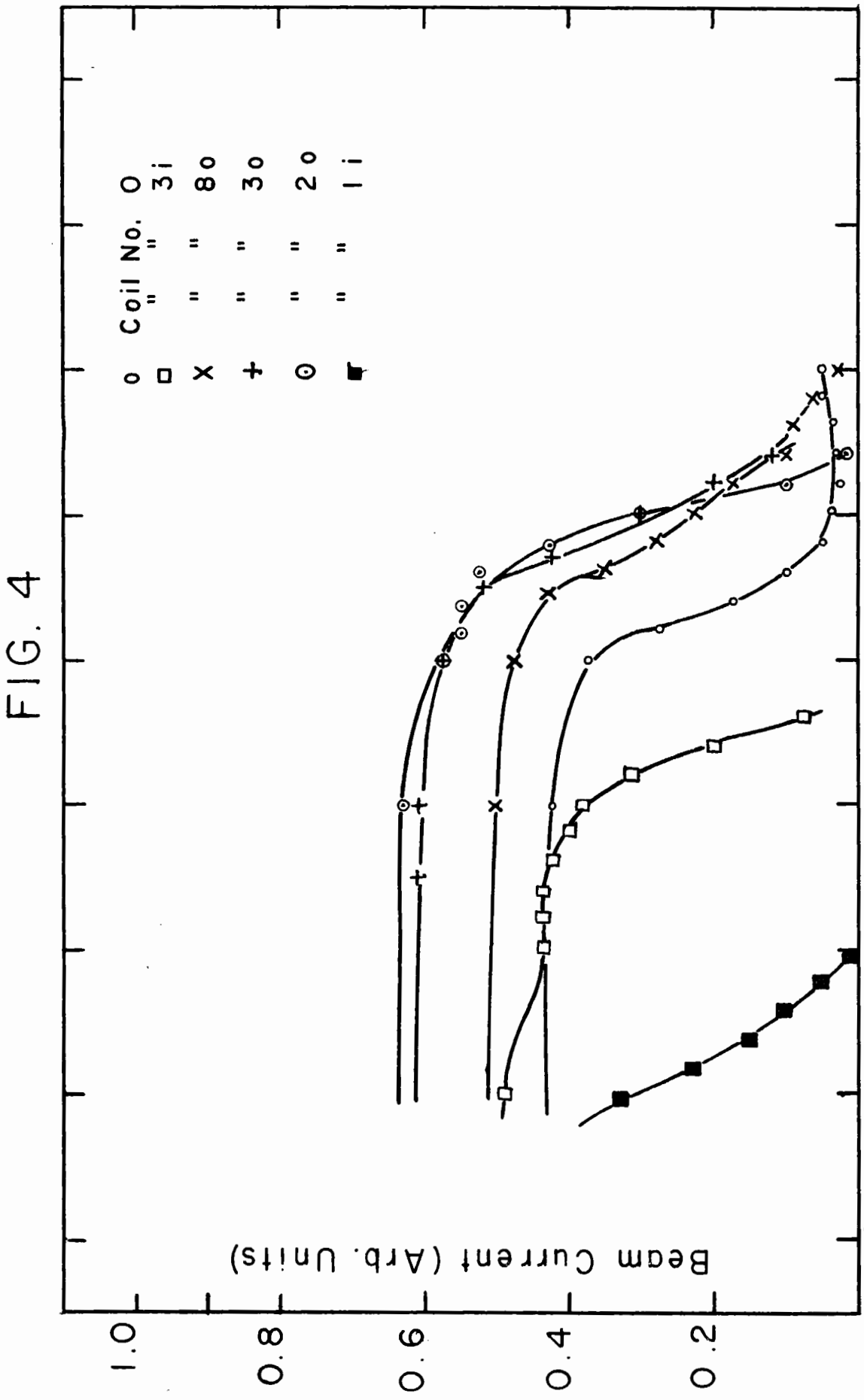
Coil No. 0
" 3i
" 8o
" 3o
" 2o
" 1i
Beam Current (Arb. Units)
1.0
0.8
0.6
0.4
0.2
30
31
32
33
34
35
36
37
Radius (Inches)
COIL SHUNTS

FIG. 4

FIG. 5

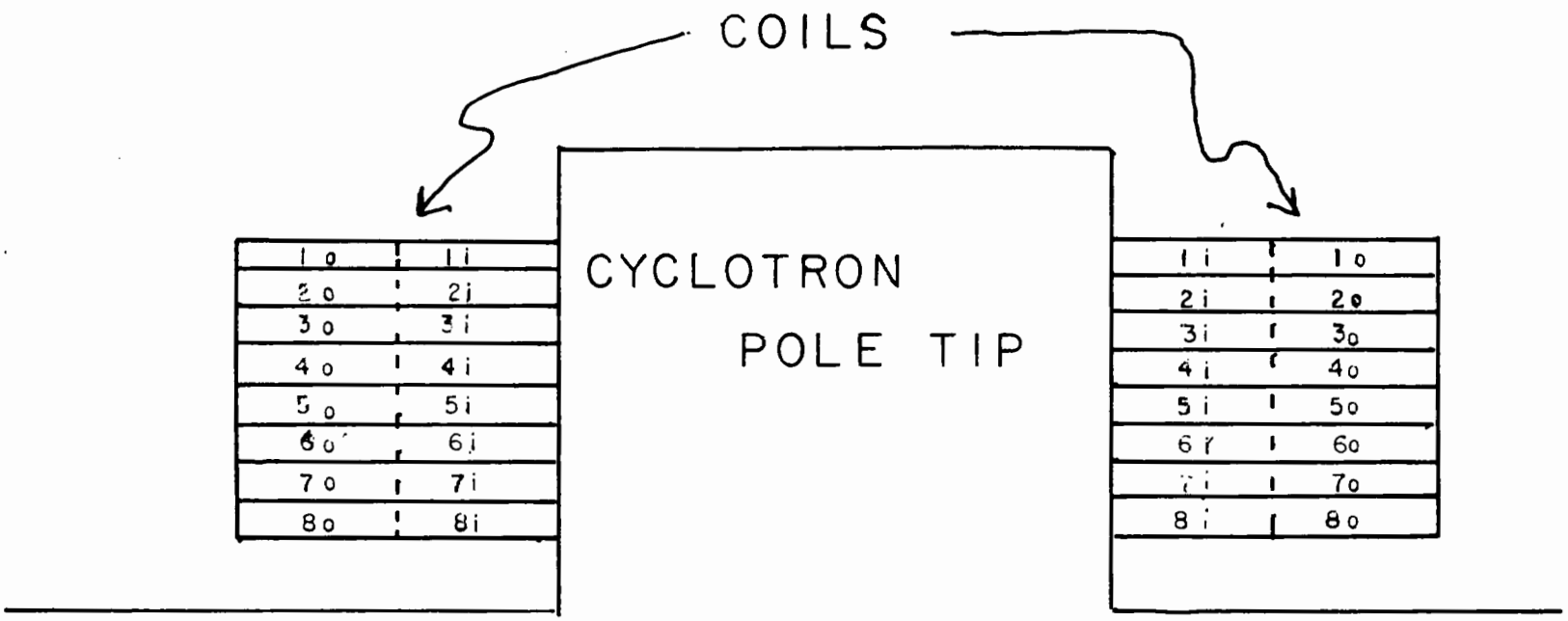

COIL NUMBERING SYSTEM

between them. Moreover, a variety of wedge shapes can be used and the radial position of the wedges can be readily and accurately determined. It was found that these wedges improve the focussing and at the same time, by slightly increasing the local field, steer the beam slightly to the left. By adjusting the position of the wedges and by raising the steering magnet $\frac{1}{2}$", the beam was reduced to 3" x $\frac{1}{2}$" and centrally located in the entrance aperture of the steering magnet.

4. The Steering Magnet

The replacement of the steering magnet coil was necessitated by the development of a serious short. Since a new coil had to be wound, it was decided to improve the design of the magnetic circuit at the same time. Since the core of the magnet was saturating, it was decided to place more iron in it and more turns were added to the coil to allow for possible widening of the air gap.

The new coils were made in four annuli. Three of these were identical, being composed of six layers of 0.105"x 0.345" rectangular wire with a total of 275 turns per annulus. The fourth annulus had four layers of the same wire and a total of 180 turns. This gave the new coil a total of 1005 turns.

A set of five cooling sheets were made. They were annuli 1/8" thick, consisting of alternate annuli of copper 3/4" wide and two 1/8" copper tubes soldered together as indicated in Fig. 6. The coils were sandwiched between the cooling sheets. The thermal contact between the sheets and the coils was provided by a layer of linseed

FIG. 6

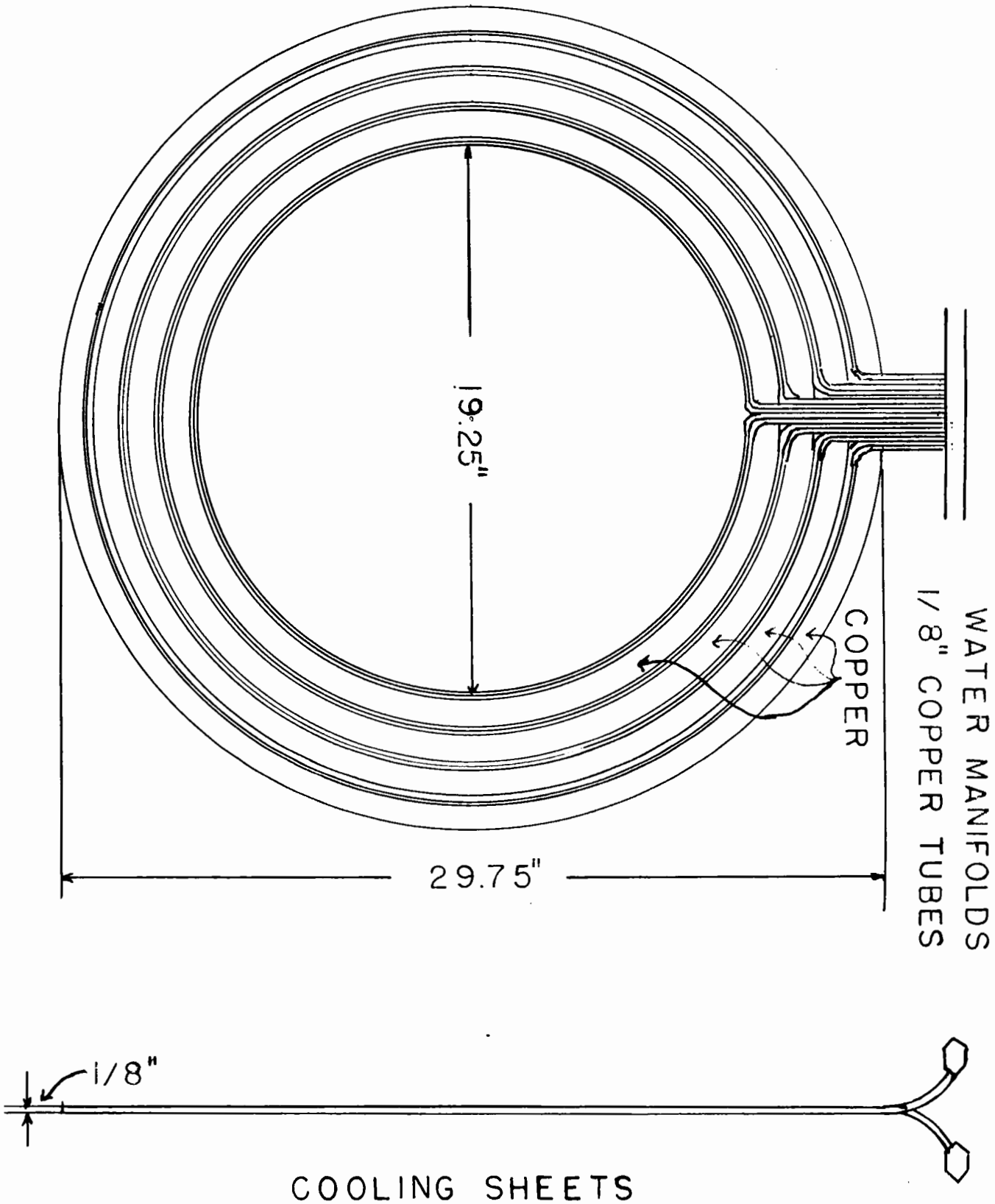
19.25"
29.75"
COPPER
WATER MANIFOLDS
1/8" COPPER TUBES
1/8"
COOLING SHEETS

oil putty, which proved to have the highest thermal conductivity of all the materials tested.

The reluctance of the magnetic circuit was decreased by increasing the iron in the core. A sleeve was made by rolling up a plate of $\frac{1}{2}$" armco iron. This sleeve was slipped over the existing core, adding 10% more iron to the core.

The comparison between the old and the improved magnet is shown in Fig. 7. The current to bring the beam out has been reduced from 53 amps to 42 amps. This 20% reduction in the current required to bend the beam with only a 5% increase in the number of turns must be attributed to the increased amount of iron in the core which therefore reduces its saturation.

The reduction in current eases the cooling problems and makes the cooling system which was set up to handle 6Kw more than adequate to handle the 2.5 Kw which is now dissipated. The cooling system further allows a much greater current to be used in the future if necessary.

FIG. 7

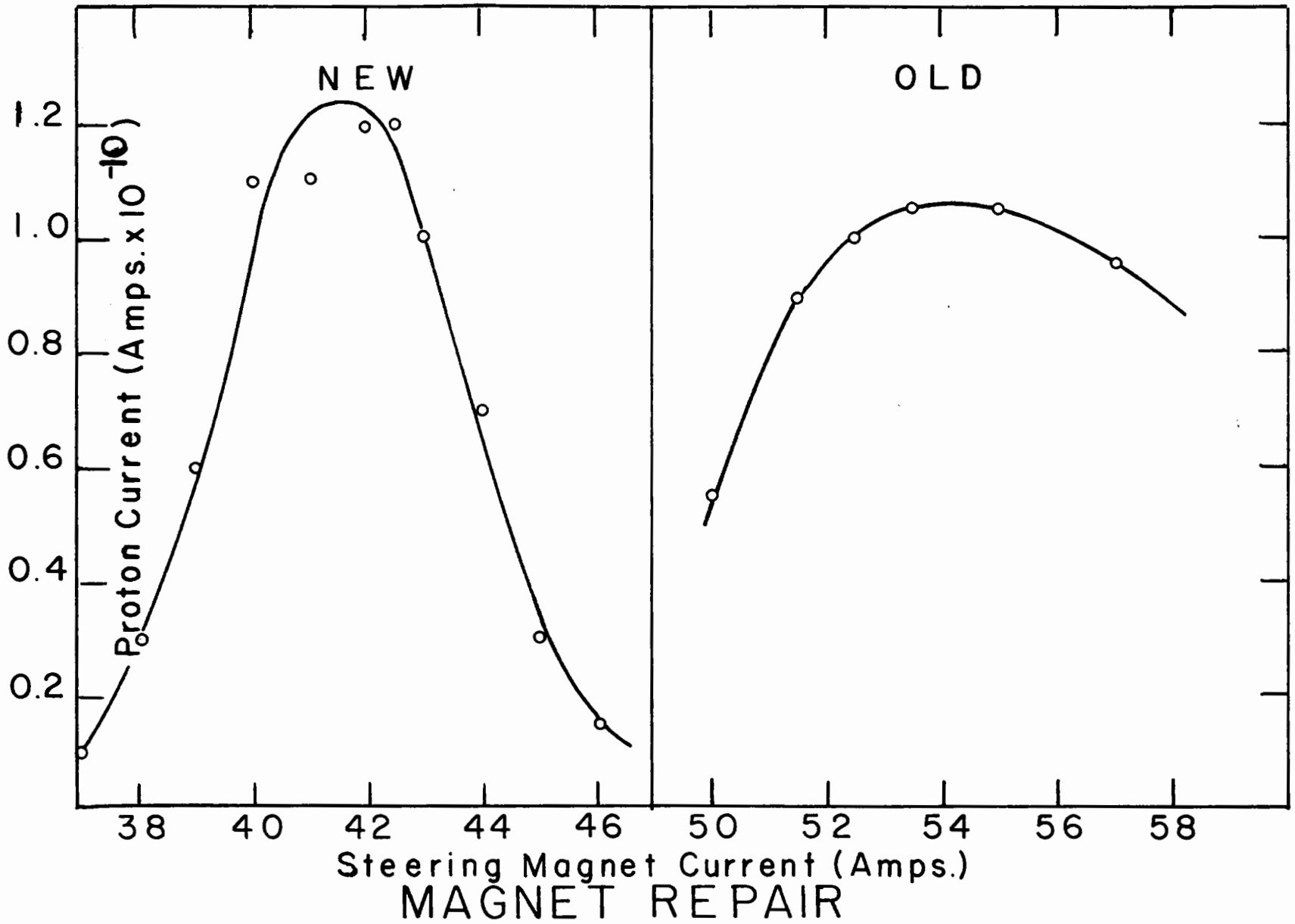

MAGNET REPAIR

5. The Final Beam

The beam at the entrance to the castle was investigated using X-ray film. Its shape was roughly a 2" x 3/4" rectangle with its long axis in the horizontal plane. The current, as a fraction of the internal beam, was measured to be 1.31×10^{-4}. That is, for one microampere internal beam the external beam would be 1.31×10^{-10} amps.

The beam was too spread out for practical use so it was reduced by collimators to a square 3/4" on a side. The current through this area was measured to be 0.4×10^{-4} times the internal beam.

The energy and energy spread of the external beam were measured by finding the cutoff point of the protons with aluminum absorbers. The current as a function of absorber thickness is shown in Fig. 8. The point at which the current is reduced to 1/2 its plateau value is 8.29 gms/cm^2 of aluminum which corresponds to an energy of 90.6 Mev. Analysis of the straggle leads to the assignment of the full width at half maximum of the energy spread of the beam as 1.17 Mev. on the assumption that this spread is gaussian.

The necessity of using the beam at all energies requires the degradation of the beam by means of absorbers. This degradation of the beam causes an increasing energy spread in the beam. An analysis of this system using the method of Link[14] is shown in Fig. 9. It is seen that the energy spread, which is defined as the full width at half maximum of the assumed gaussian,

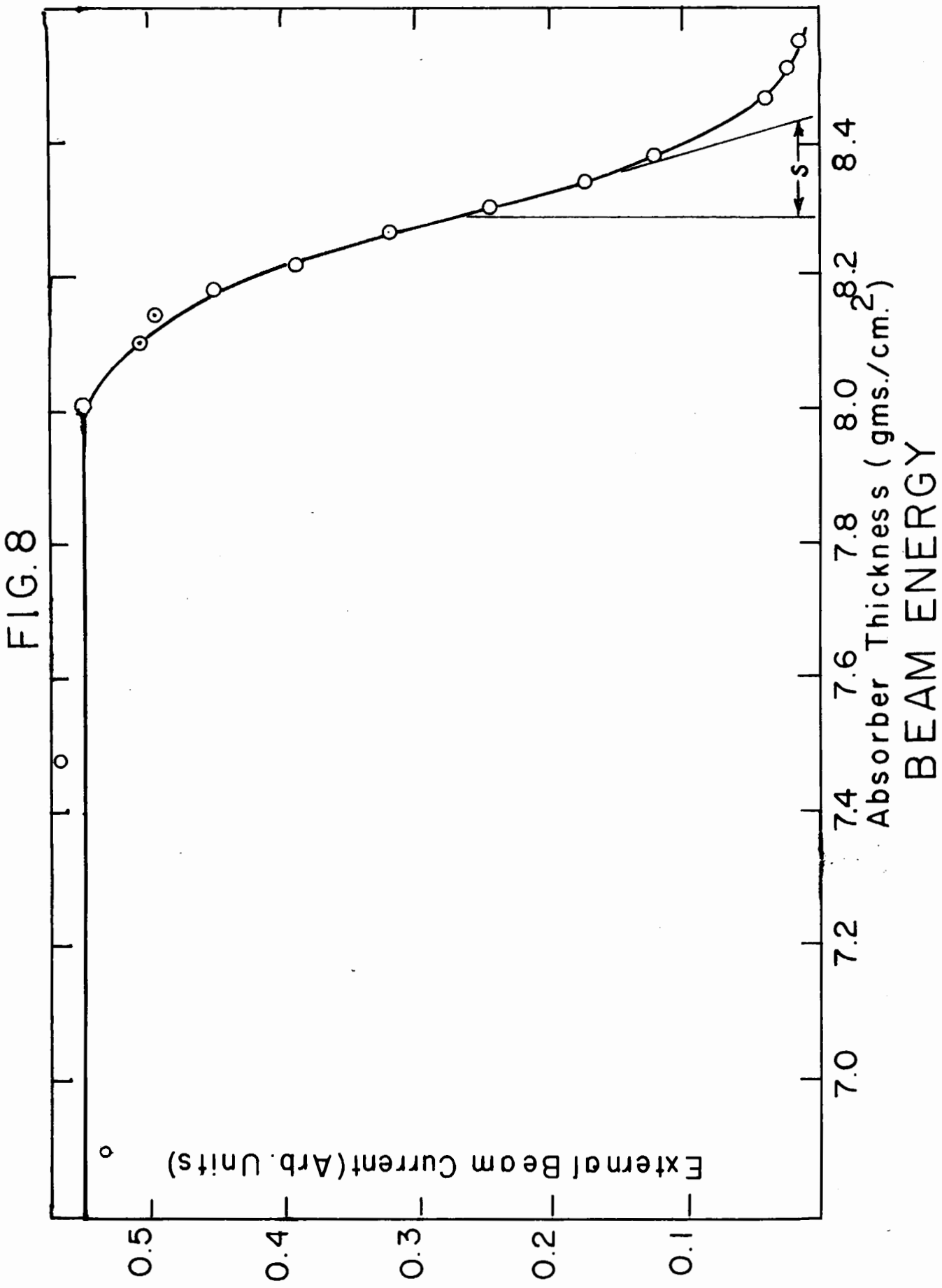
External Beam Current (Arb. Units)
0.1
0.2
0.3
0.4
0.5
7.0
7.2
7.4
7.6
7.8
8.0
8.2
8.4
Absorber Thickness (gms./cm.²)
BEAM ENERGY
S

FIG. 8

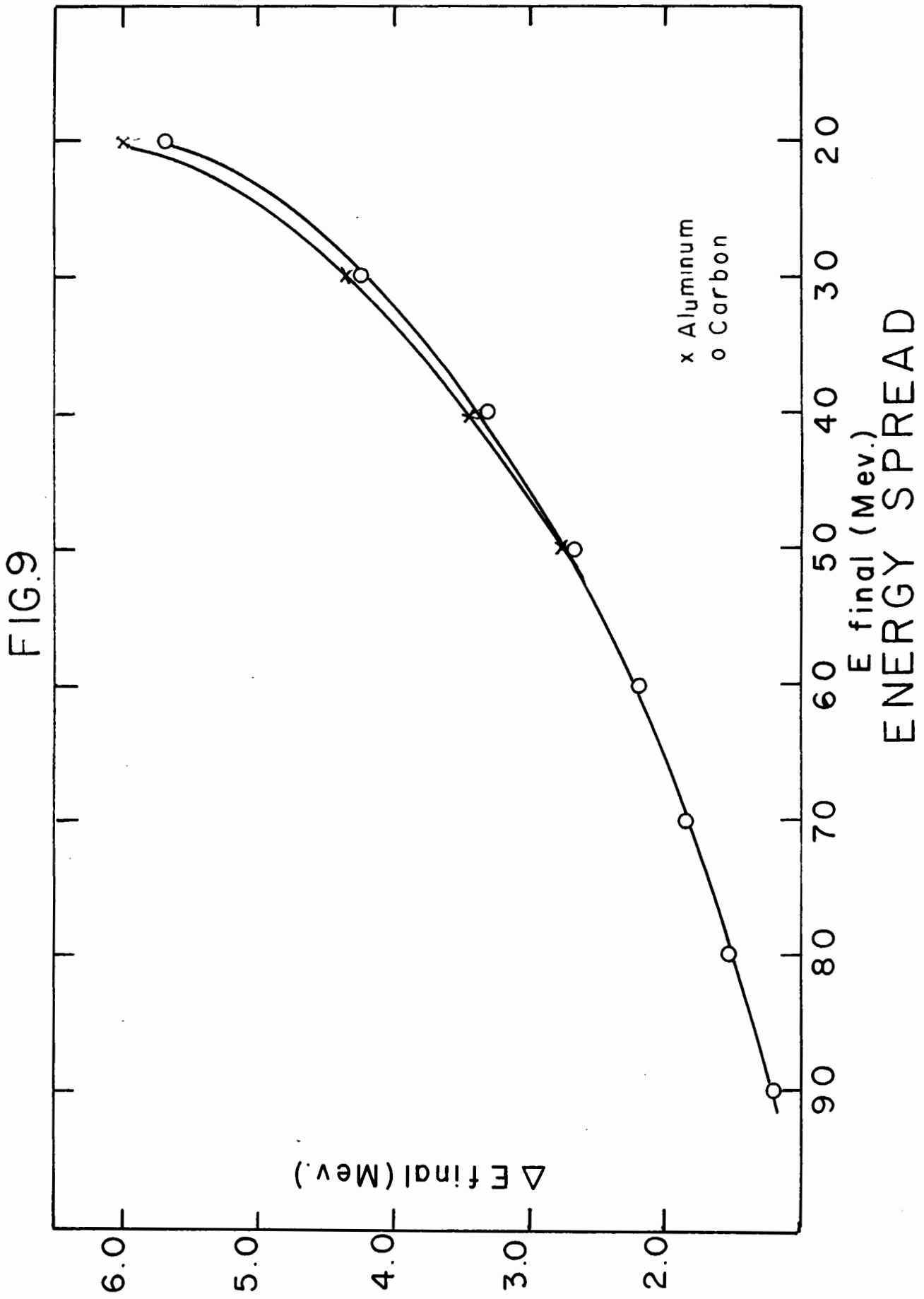
FIG.9
ENERGY SPREAD
E final (Mev.)
ΔE final (Mev.)
x Aluminum
o Carbon
6.0
5.0
4.0
3.0
2.0
20
30
40
50
60
70
80
90

for 20 Mev protons is 5.7 mev. The beam is also spreading in angle due to the scattering of the protons as they are sent through the absorbers. This effect makes it difficult to determine the current through the target at one energy relative to another.

CHAPTER II

CIRCUITRY

The instrumentation is designed to measure the time of arrival of gamma-rays from a nucleus in the target relative to the passage of the burst of protons through the target. This is done by switching gamma-ray pulses into seventeen integrators in succession for equal lengths of time. The basic units in this system are the integrators and the switching circuits.

The integrators are copied from a design by R.E. Bell. The switching circuits for these integrators are built around two magnetron beam switching tubes. Each of these tubes consists of a single cathode and ten identical sets of electrodes arranged around the circumference of a circle. Each set consists of a grid, an anode and a "spade" electrode. Voltages on these electrodes are arranged so that the entire electron current goes to one section. Timing pulses on the grids cause the beam to switch from one section to the next in 0.1 μsec. The section on which the electron beam "dwells" selects the integrator into which the gamma-ray pulses go. The time which the electron beam "dwells" on each section of the beam switching tubes and consequently the counting interval for each integrator is set by the repetition rate of pulses from a crystal-controlled time mark generator (Tektronic Type 851).

A target placed in the external beam is bombarded with bursts of protons of approximately 20 μsec duration and (if

uninterrupted) at a regular repetition rate of 400 per sec. The cyclotron is triggered by pulses at this repetition rate which pass through a gate circuit. After the gate is opened the next triggering pulse will turn on the cyclotron oscillator and after a further period of 400 μsec (the cyclotron acceleration time) a proton burst strikes the target. The circuitry described here is designed to study the distribution of the gamma-rays in time and energy which come from the target after the passage of the proton bursts.

A block diagram of this circuitry is shown in Fig. 10. The beam is detected by a plastic scintillator backed by a photo-tube. The output of the detector is amplified and integrated to measure the beam intensity. Also, the amplified output activates a scaler. The scaler is modified to give an output after counting a set number of pulses (1, 2, 4,.....64). A delay D1 is started by the scaler and the cyclotron gate is closed. The delay is imposed to remove any unavoidable short-lived activity. At the end of the delay the phototube is turned on and the Beam Switching Tube is activated by turning on the Time Marker Generator. When the end of the last counting period has been reached, an output from the Beam Switching Tubes stops the Time Marker Generator, closes the phototube and initiates a second delay D2. The second delay is used to regulate the period of the sequence which is D1 plus the counting interval plus D2. This regulation is necessary to prevent the buildup of long-lived radioactive decay. At the end of D2 the cyclotron gate is opened, allowing the next occurring

FIG. 10

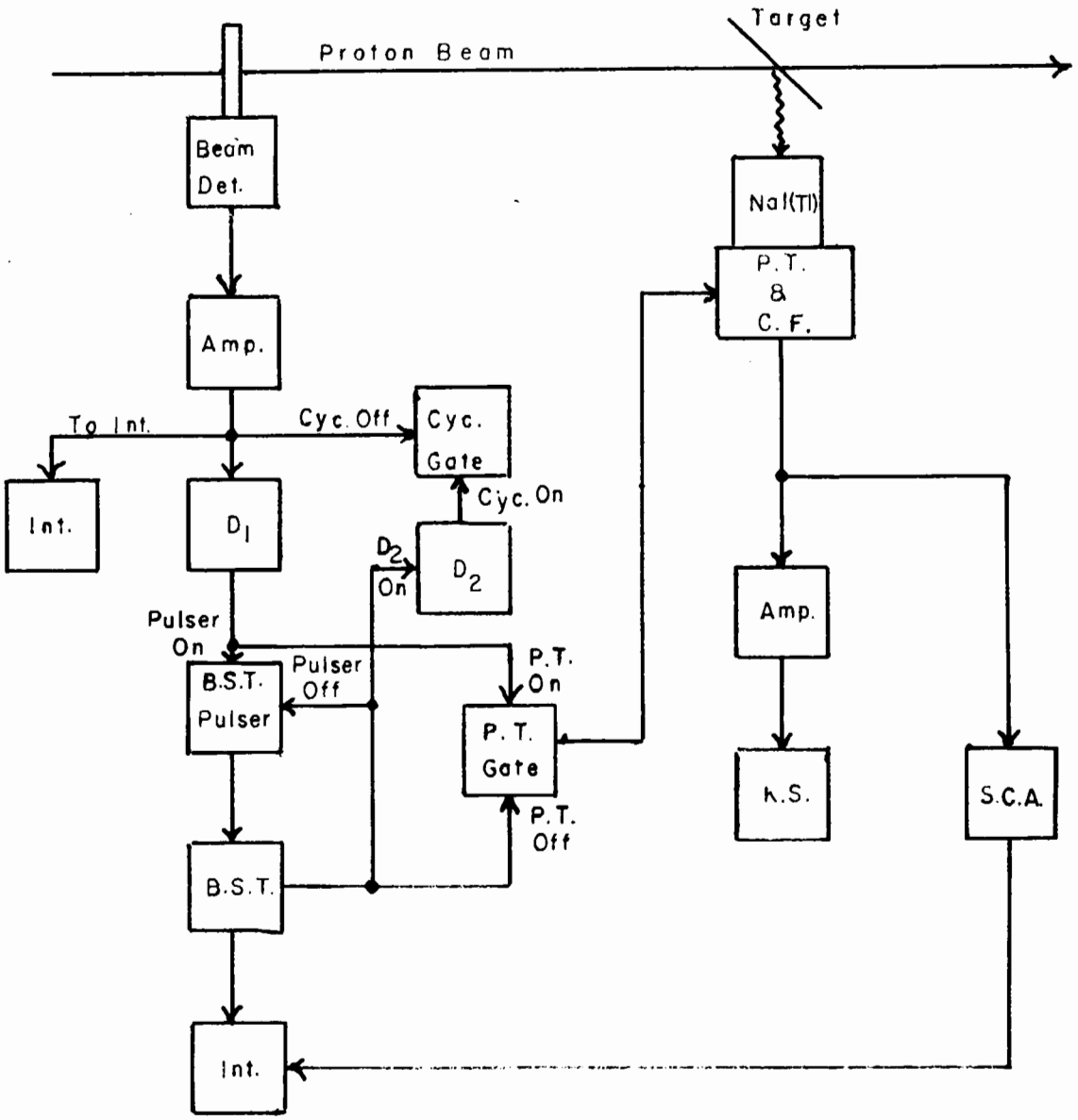

BLOCK DIAGRAM
OF ELECTRONICS

FIG. 11

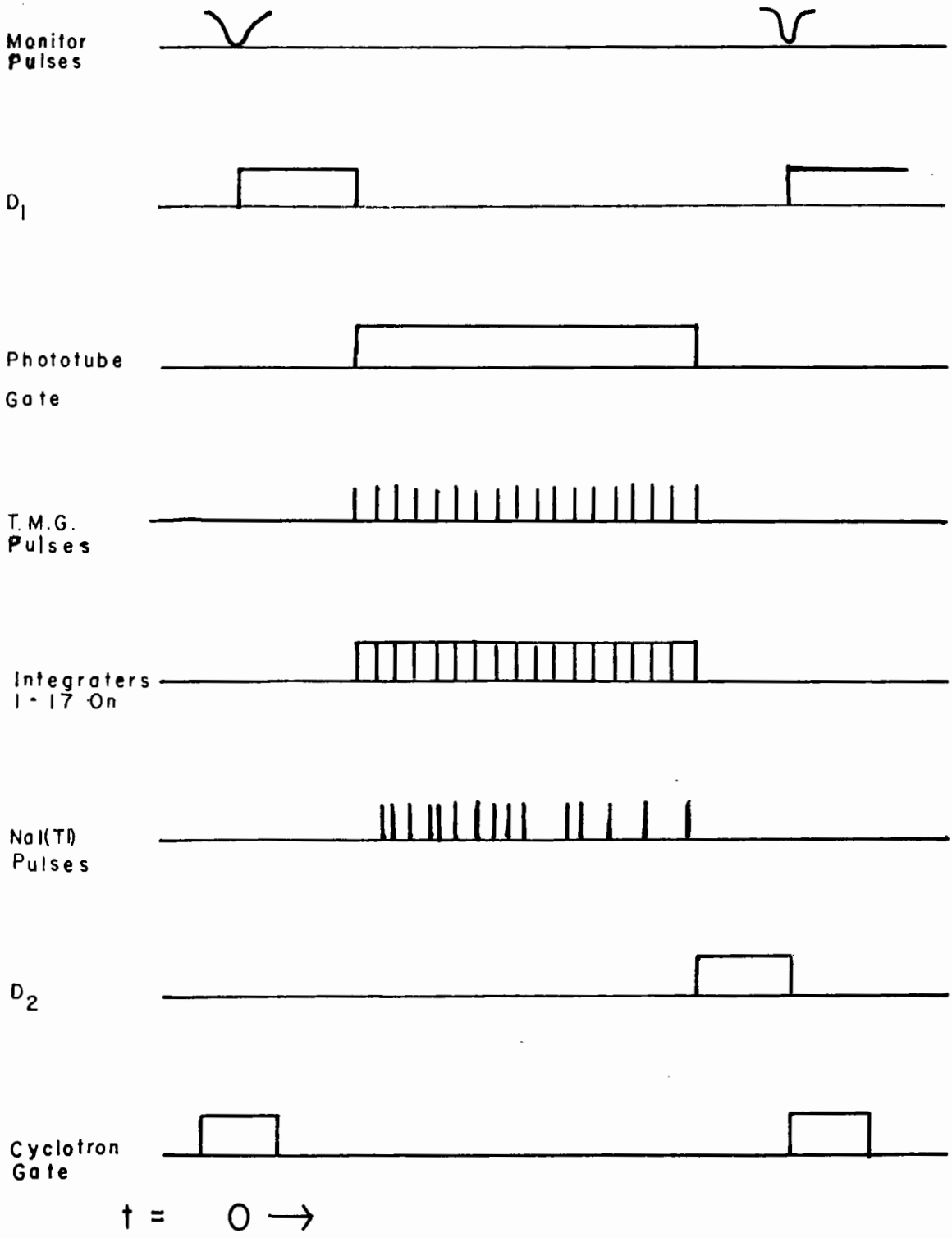

TIME SEQUENCE

cyclotron trigger to pass and the sequence repeats itself. The sequence of these various operations is shown in Fig. 11.

The gamma-rays from the target are detected by a $1\frac{1}{2}$" x $1\frac{1}{2}$" NaI(Tl) crystal whose phototube gating circuit and cathode follower were built by W.T. Link[14]. The output from this detector is sent to an amplifier and a 256 channel kicksorter and also to a single channel analyzer. The single channel analyzer can be connected in coincidence with the kicksorter to allow a quick check on its energy range. The output from the single channel analyzer is sent to the integrators where its distribution in time is checked. The use of this device also allows us to check the time spectrum of any part of the energy range. The details of the circuitry are discussed in Appendix I.

CHAPTER III

BACKGROUND

A serious difficulty in the detection of the isomeric states was the high number of background counts. This high background was composed of a short-lived component with a half-life of about 50 μsec and a longer-lived component of between 125 and 200 μsec. The long-lived component was ascribed to the thermalization of neutrons, produced by the slowing down of and stopping of the beam by the absorbers, target and the beam sink.

An attempt was made to reduce the long-lived component by slowing down and capturing the neutrons quickly in the area of the target. The target was surrounded by a saturated solution of borax and water. This mixture was calculated to capture neutrons with energies up to 2 or 3 Mev in about 20 μsec. However, the background was increased by this measure and this was explained on the assumption that many of the neutrons were produced at much higher energies which allowed them to punch through the water and bounce around until they were thermalized. They would then be very strongly absorbed in the borax thereby creating a delayed high activity near the crystal.

Since it was not feasible to build a tank large enough for the prompt absorption of high energy neutrons this system had to be replaced. Since a light material had proved unuseable in these conditions a heavy castle had to be built. Lead had proved unsuitable because it contained many isomeric states which could be excited either by fast neutrons or protons. These isomeric

states increased the background above useable levels. Iron seemed the most likely material. It was given a preliminary test which showed no troublesome short-lived activities. Therefore an iron castle was constructed.

A test was made to determine the best position for the castle in the corridor. The relative background was measured as a function of position across the corridor. The result of this measurement is shown in Fig. 12. There is a broad minimum near the centre of the corridor and this is where the castle was located.

The castle was built in the shape of a hollow cube with its inside edge 18" long and a wall thickness of 5". This left a large space around the crystal. This was necessary to reduce the backscatter peak which is very prominent in low Z materials.

The instantaneous counting rate for all γ-rays above 50 Kev and 50 μsec after the passage of the beam was measured to be 338 cps. It decayed with a half-life of 150 μsec. This is to be compared with a similar measurement by Link of 1500 cps in which his beam was one sixth the present beam. His castle also had a 50 μsec activity which was absent in this case. Therefore the iron castle fulfilled the requirements and was used in all the experiments which follow.

FIG.12

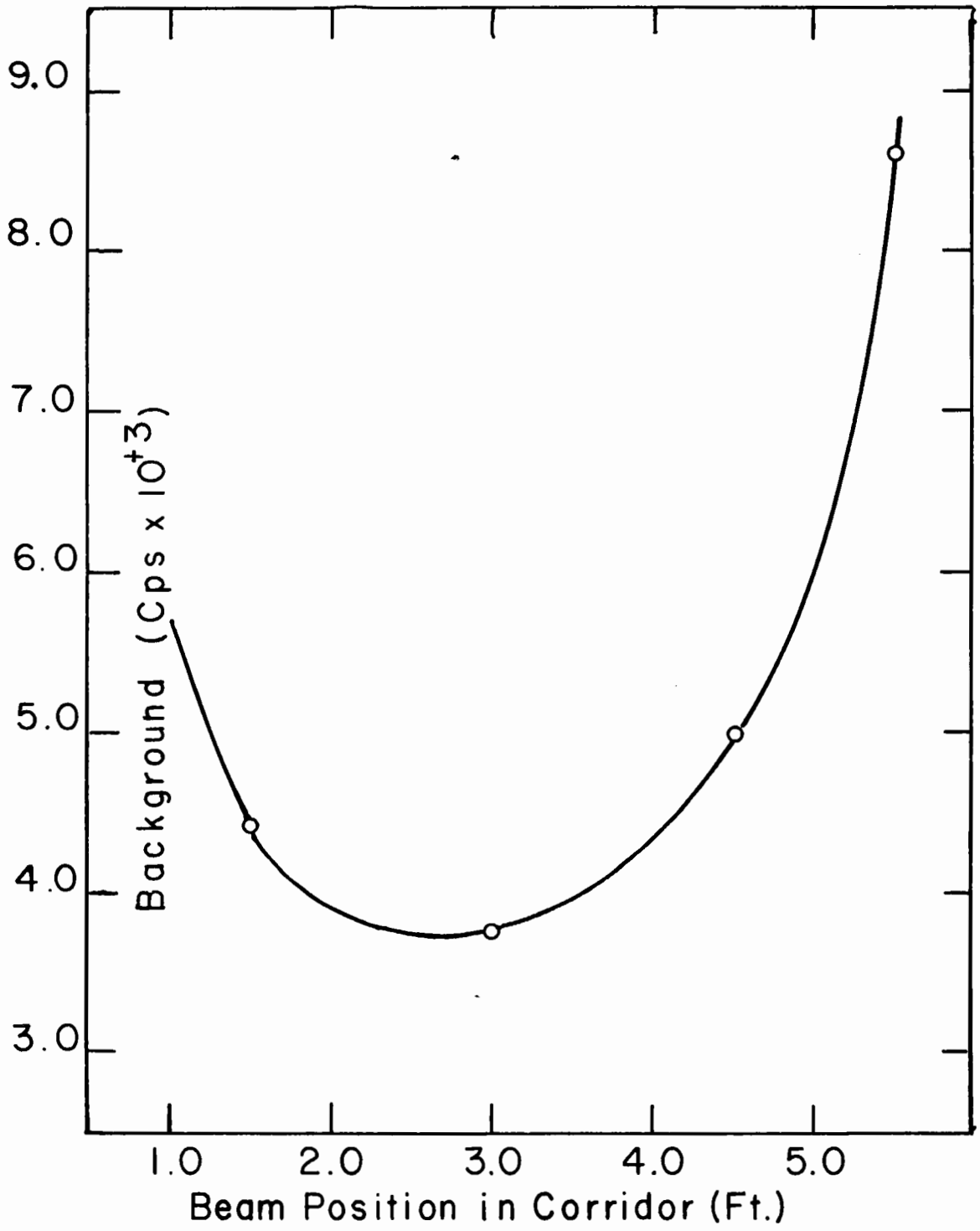

CORRIDOR BACKGROUND

CHAPTER IV

EXPERIMENTAL METHODS

A brief discussion of the experimental methods is given in order to show the general pertinence of the measurements taken. The quantities which describe an isomeric state are:

1. The atomic number of the nucleus.
2. The mass number of the nucleus.
3. The energy of the isomeric state.
4. The spins and parities of the energy levels of the nucleus.
5. The half-life of the isomeric state.

The determination of the atomic number for an isomer may be made in two ways. The first and most exact way is by critical absorption of the associated X-rays if they are available. An experiment of this type demands an X-ray energy high enough to be detected by a NaI(Tl) crystal and is therefore satisfactory for $Z > 36$. The accuracy of these experiments is limited by the counting rates of the X-rays which are generally quite low. These counting rates are such that the crystal must be quite close to the target and hence the yield of absorber characteristic X-rays is high enough to reduce greatly the accuracy with which the attenuation of the absorbers may be determined. However, this only makes quantitative calculation of the absorption difficult. The changes of X-ray intensity from one absorber to the next are still decisive.

The second method of measuring the atomic number is through the shape of the cross-section curves. This method is reliable for high Z'S only.(31,32) This is because the high Z of

the nucleus tends to inhibit the emission of a proton. Therefore the (p, xn) reactions tend to have much higher cross-sections than the (p,pxn) reactions. The second fact which distinguishes between these two reactions is the shape of the curves. The (p, xn) reactions are very sharply peaked and are followed by a very weak tail which extends well beyond the maximum. The (p, pxn) reactions are not only much weaker, they also do not have a sharp maximum and they drop off only very slowly as the energy rises. Therefore, a measurement of the shape and magnitude of these curves in the heavy element region usually provides a very good check on the Z of these elements. The details of these curves are much less well known for the lower Z elements and consequently the results would be much more ambiguous. Also, the fact that the coulomb barrier is much smaller removes the distinction due to the sharp peaking between the (p, xn) and the (p, pxn) reactions.

The measurement of the mass number of the nucleus is confined to a knowledge of the cross-section and most of the remarks which apply to the measurement of atomic number also apply here. The fact that the (p, pxn) reactions are not sharply differentiated one from another, combined with the fact that the degraded beam has a fairly large energy spread, makes the "A" sharply determined only for the (p, xn) reactions on high Z materials.

The energies of the levels involved can be measured as accurately as the NaI(Tl) crystal will allow. This is probably the most accurately measured quantity. It is, however, subject to the limited resolution which tends to hide any close peaks and may

give false results in the measurement of an energy due to the distortion of a peak. Also any low lying peaks may be hidden in the Compton distribution of the higher peaks and make impossible the determination of the decay scheme. This last effect is not likely to be too large since when a level de-excites it does it in as short a method as possible, which tends to remove complex decay schemes. However, highly converted low energy states may be missed because of this effect and there are several examples of this happening.

The spins and parities of the levels can be determined under ideal conditions only, because not enough information is available. The facts which we can get that relate to this are the relative intensities of the gamma-rays and K X-rays, and the half-life of the state. The most important measurements are the relative intensities of the states which, in principle, can be measured quite accurately for ideal conditions with a NaI(Tl) crystal. For simple cases in which there are one or two gamma-rays, this is done, but with complex spectra with many branching ratios this is not possible. In our experiments the measurement of the relative intensities is complicated by the large source. The efficiencies of the counter have been measured for a point source at a fixed distance and these efficiencies have then been used to calculate the relative intensities, directly from the broad source. This assumes that the relative efficiencies for the gamma-rays is not much affected by the broadening of the source and the different distance of different parts of the source which is at 45° to the axis of the counter. Undoubtedly, this is

not accurately true and probably introduces 5 - 10% error into this calculation. The error would be even greater in the measurement of the absolute intensity of any of the gamma-rays.

In simple decay schemes, the measurement of the relative intensities of these gamma-rays gives us a measure of the conversion of the various gamma-rays. A comparison of these conversions with the calculated conversion coefficients allows us to assign the multipolarities of the converted gamma-rays fairly accurately. The weakly converted gamma-rays are completely unidentifiable in this scheme and can only be fitted by comparison with known decay schemes and with the almost infinite flexibility of the shell model.

The half-life of the isomer is measured fairly accurately with the instrumentation previously described, providing there is no long-lived high intensity background from the target or from the background of, say, the counting castle. Then the fact that there are only seventeen channels makes it impossible to follow this background long enough to make an accurate subtraction. This is not really a great deterrent to the determination of the decay scheme since the theoretical predictions of the Weisskopf estimates differ by a factor of 10^3 or 10^4 from the measured values, except for M4 transitions.

CHAPTER V

RESULTS

(a) Po^{205m}

1. Experiments

An isomer was discovered in Po^{205} by W.T. Link when he bombarded bismuth with protons at 50 Mev. It was characterized by a 707 Kev γ-ray and its X-rays decaying with a half-life of 644 μsec. It was decided to re-examine this isomer with the hope of finding a new gamma-ray in the spectrum.

A second γ-ray was found in the spectrum close to the backscatter peak of the 707 Kev γ-ray at 160 Kev. The new castle with its reduced backscatter peak is responsible for this discovery.

With two peaks in a decay, it is necessary to show they decay with the same half-life. This proof is difficult for our weak γ-ray since it is superimposed on the high Compton of the 707 Kev γ-ray and the long-lived background. However, if its intensity relative to the 707 Kev γ-ray remains the same when the delay of the counting period is changed, then its half-life is established to within the accuracy of the measurement of the relative intensity. This experiment was done with the same target of 0.013" Bi, a counting interval of 680 μsec and delays of 50 and 500 μsec. The results are as follows:

TABLE I

DELAY	RELATIVE INTENSITY
sec	%
50	6.8 ± 1
500	6.8 ± 1

The close agreement is fortuitous, but it does indicate that the intensities of the two γ-rays decay at the same rate, as will be assumed in the following discussion.

The energy spectrum is shown in Fig. 13. The strong 707 Kev γ-ray and 80 Kev X-ray are the main features of it, with weak peaks at 160 Kev and 480 Kev. The 160 Kev γ-ray is not much stronger than the Compton on which it is superimposed. An attempt was made to remove the Compton by subtracting the 662 Kev γ-ray spectrum of Cs^{137} from the spectrum of the 707 Kev γ-ray by changing the gain of the kicksorter amplifier until the two peaks are superimposed and then subtracting the Cs^{137} spectrum until the 707 Kev peak has merged with background. The shape of the Cs^{137} Compton is not altered much by this gain change except that the back-scatter peak occurs 7% too high. This leaves behind any weak γ-rays and the natural background. The result of this subtraction is shown in Fig. 14. The raggedness of the points is caused by the large statistical fluctuations inherent in such a subtraction process. The 160 Kev γ-ray is strongly emphasized and a weak peak at channel 65 also appears. This is at the maximum part of the Compton edge of the 707 Kev γ-ray and a little below the 511 Kev of energy released by

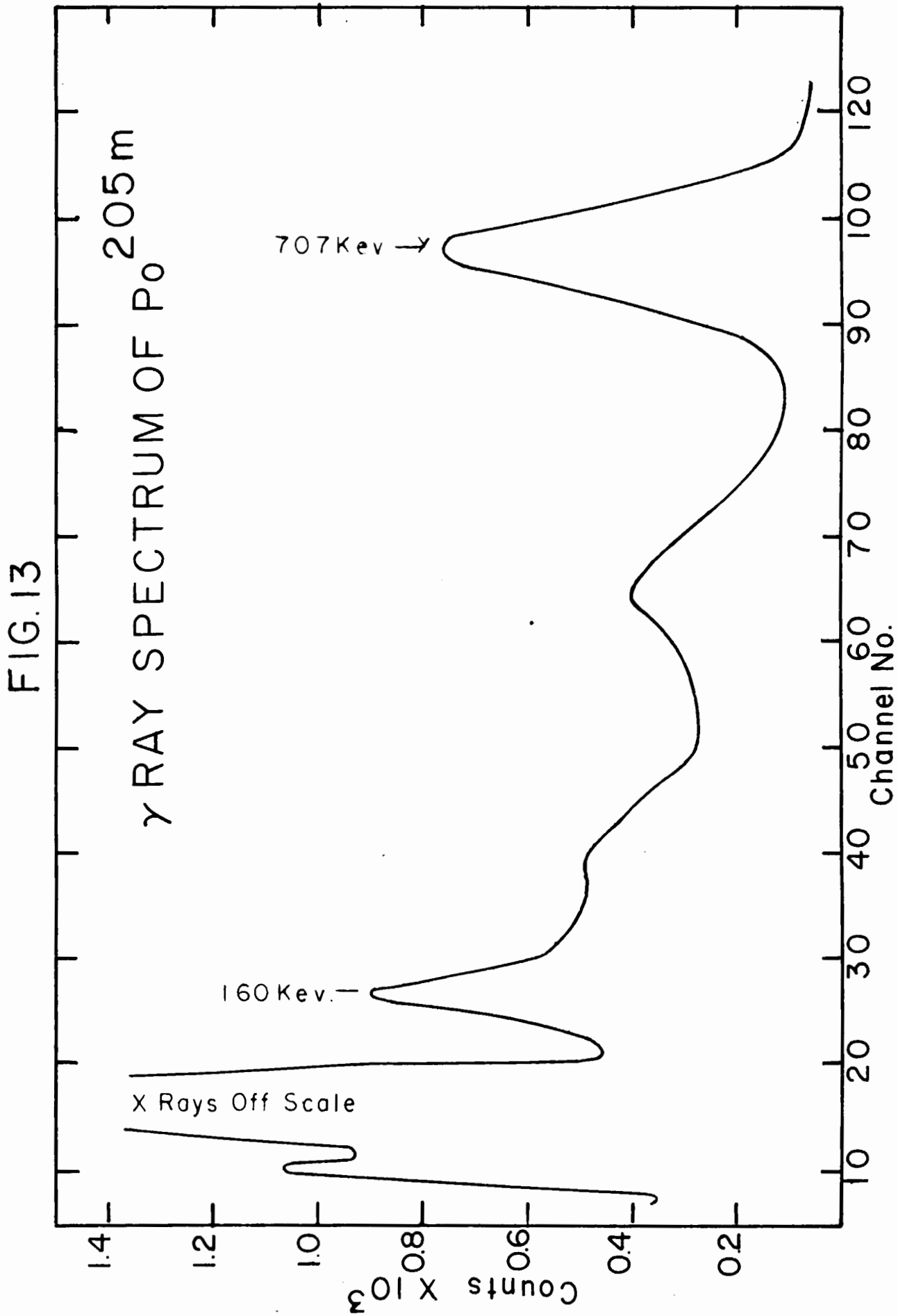
γ RAY SPECTRUM OF Po 205m
707Kev
160Kev.
X Rays Off Scale
Counts X 10³
Channel No.
1.4
1.2
1.0
0.8
0.6
0.4
0.2
10
20
30
40
50
60
70
80
90
100
120

FIG. 13

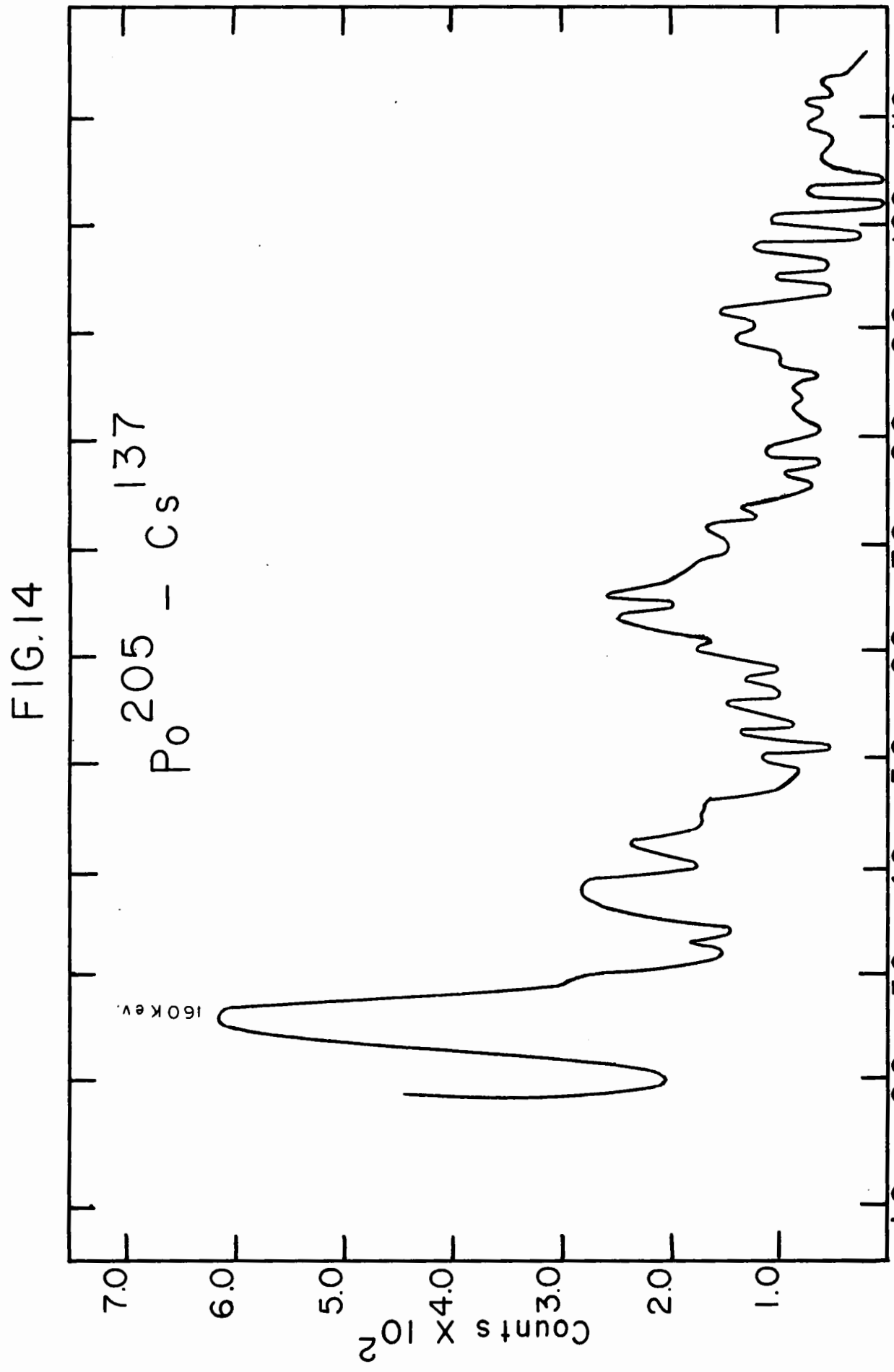

FIG. 14

$Po^{205} - Cs^{137}$

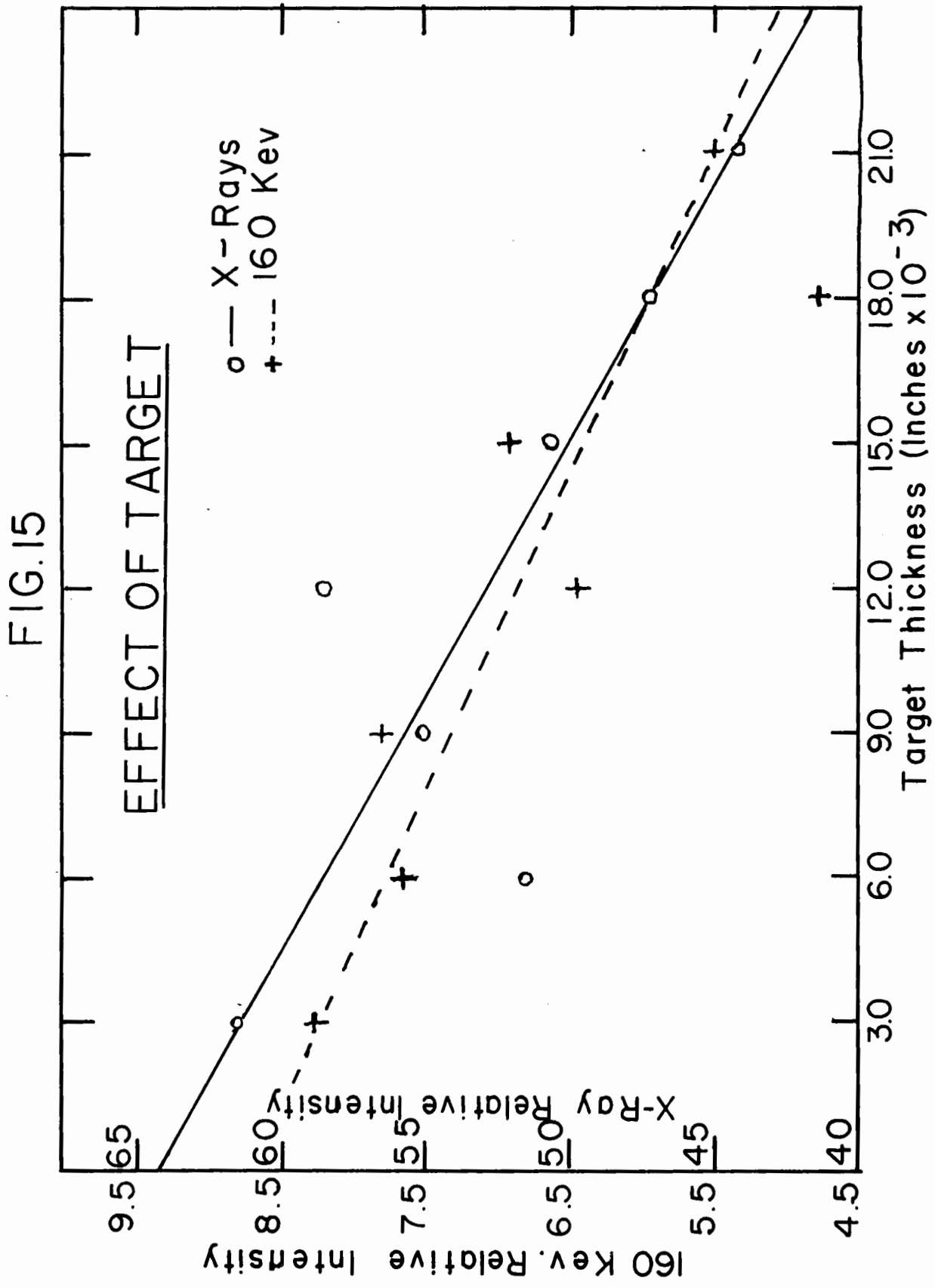
FIG. 15
EFFECT OF TARGET
o — X-Rays
+ --- 160 Kev
160 Kev. Relative Intensity
X-Ray Relative Intensity
Target Thickness (Inches x 10^-3)
9.5
8.5
7.5
6.5
5.5
4.5
65
60
55
50
45
40
3.0
6.0
9.0
12.0
15.0
18.0
21.0

positron annihilation. The annihilation radiation is always present in the background. The positrons are produced by the long-lived decay of iron activated by the scattering of protons from the beam into the castle and by pair production from high energy γ-rays from neutron capture in the surrounding materials. These two effects do not seem to account completely for this peak or the broad peak immediately prece ding it. These may be weak γ-rays associated with the decay, but if such is the case they are too weak to allow any analysis. It is possible that they constitute a weak parallel decay route.

The new information which is obtained from this spectrum is the relative intensities of the X-rays and the γ-rays. To measure the intensity of the X-rays and the 160 Kev γ-rays the target thickness had to be taken into account. Their intensities were measured relative to the 707 Kev γ-ray which would not be affected by the target thickness for the reasonable values used. The results are shown in Fig. 15. The X-ray statistics are considerably better than those of the 160 Kev γ-ray since the intensity of the X-rays is high compared to background. The scatter in the points is due to the low number of counts under the peak for the thin targets.

The 160 Kev γ-ray results are subject to quite large statistical errors due to the large Compton on which they are standing. An error was introduced by the subtraction method in the position of the backscatter peak. The gain change moved this 7% too

high. Since the backscatter peak of the 707 Kev γ-ray is not resolved from the 160 Kev γ-ray, this 7% shift will mean that not enough counts are subtracted from the 707.

The backscatter peak of the 707 Kev γ-ray occurs at 187 Kev. The backscatter peak of the 662 Kev γ-ray with its photopeak superimposed on the 707 Kev γ-ray occurs at an effective value of 197 Kev. The backscatter peak of the 662 Kev γ-ray occurs at 185 Kev. This value of 185 Kev is close enough to that of the 707 Kev γ-ray backscatter peak that the two may be considered the same energy. The shape of the Compton distribution is similar enough to allow the Cs spectrum under the backscatter peak to be subtracted from the Po spectrum with the 662 peak height normalized to the 707, to determine the intensity of 160 Kev γ-ray. This subtraction was done and the number of counts under the photopeak was found to be 712. The number under the same peak with the subtraction done, with the gain of the amplifier changed, was 1203. Since the gain changing method was much simpler, all intensities were measured using it and the final intensity was reduced in the ratio 712/1203.

Although an attempt was made to keep all subtractions consistent, it is possible for quite large systematic errors to occur at this stage. The counting rates were quite small so that the statistical errors were large and this is shown in the large scatter of the points. The results are consistent within the probable experimental errors. Another consistency in the results is the slope of the absorption curves. It just happens that 160 Kev and the X-rays

have the same absorption coefficients and therefore the two curves should have the same slope, which they do within the experimental error.

With these corrections taken into account, and also corrections to the X-rays of 5% for the Auger effect, the measured relative intensities are:

TABLE II

γ-ray Energy	Kev	707	160	X-rays
Intensity	Arb. Units	100	5.2	64

From these figures and the known conversion coefficients, we can attempt to assign the multipolarities of the γ-rays.

2. Analysis

To analyse the decay we must assume that there are no unobserved transitions or, if there are unobserved transitions, that they are too weak to affect the conclusions. The second assumption that we must make is that the 160 Kev γ-ray and the 707 Kev γ-ray are in cascade. Under these assumptions there are two possibilities.

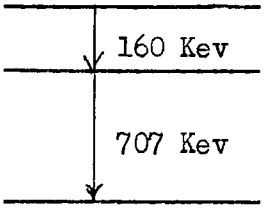

(1)

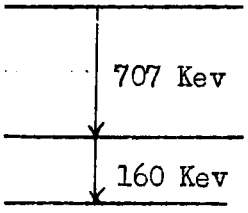

(2)

For the purposes of this discussion the subscript 1 will refer to the 160 Kev γ-ray, and subscript 2 to the 707 Kev γ-ray.

In either case the following situation is demanded:

$$I_1 (1 + \alpha_1) = I_2 (1 + \alpha_2) \qquad (1)$$

where the I's refer to the relative intensities of the γ-rays and the α's are their total conversion coefficients.

A further relation that is necessary is that the X-ray intensity must be the sum of the conversion of the two γ-rays, i.e.:

$$I_1 \alpha_{K1} + I_2 \alpha_{K2} = I_{K\ X\text{-ray}} \qquad (2)$$

These, and the Weisskopf estimates, are the main facts with which we have to work.

Case 1

In this case γ_1 is the isomeric transition and it is followed by γ_2. It is reasonable to assume that the conversion coefficients of γ_2 are small enough to be neglected, since two large spin changes are unlikely and the conversion coefficients for a γ-ray of that energy are less than 2% when the multipolarity is 2 or lower.

Therefore, equation (1) becomes

$$I_1(1 + \alpha_1) = I_2$$

Putting in the experimental values for the intensities, we get

$$\alpha_1 = \frac{I_2}{I_1} - 1 = \frac{100}{5.2} - 1 = 18.2$$

The known conversion coefficients for a 160 Kev γ-ray are:

TABLE III

Multipolarity	β_1	β_2	β_3	α_1	α_2	α_3	α_4
Total	2.95	16	76	0.13	1.15	9.8	100
K	2.2	10	30	0.11	0.27	0.6	1.4

A glance at this table shows that there is only one likely possibility, β_2. There is, however, another possibility in α_3, although it seems less likely. A decision can be made on the basis of the K X-ray conversion coefficients. If we assume that it is α_3, we see that the K conversion coefficient is 0.6, and the total conversion coefficient is 9.8. The γ-ray intensity as calculated from the total conversion coefficient would be

$$I\,(1 + \alpha) = 100$$

$$I = 100/(1 + \alpha) = 100/10.8 = 9.25$$

Using this value of the γ-ray intensity and the calculated conversion coefficient of 0.6, the K X-ray intensity would be

$$9.25 \times 0.6 = 5.6$$

This is far enough from the measured K X-ray intensity of 64 to allow us to rule α_3 out as a possibility.

On the other hand, applying the same method to the β_2 we get a calculated γ-ray intensity of 5.9. Since the K X-ray conversion coefficient is 10, the X-ray intensity would be $10 \times 5.9 = 59$. This is within the experimental error in the measured X-ray intensity

of 64. This seems to allow unambiguous assignment of the γ_1 as β_2. This, of course, does not give any indication of the multipolarity of γ_2.

Since the errors are so large in the measurement of the intensity of γ_1, it seems reasonable to use the intensity arrived at from the calculated conversion coefficient rather than the measured value. This does not remove any of the validity, since the establishment of the multipolarity is unambiguous.

A further check on the validity of this assignment is possible through the use of the Weisskopf estimates for γ-ray half-life as a function of energy and multipolarity. The half-life of this transition from the Weisskopf estimates, is not less than 0.2×10^{-5} sec. The measured value of the half-life from our experiments is, taking into account the conversion which shortens it, 11.0×10^{-3} sec.

The Weisskopf estimates give the minimum half-life for γ-ray emission. The values calculated by this method are less than the measured values except in the case of E2 multipolarities where transition probabilities are enhanced by collective effects. Transition probabilities of neighbouring multipolarities are separated by a factor of the order of 10^6. The measured values of γ-ray lifetimes are longer than their estimated values and shorter than the estimated value for the next higher multipolarity. The magnitude of the difference between the estimated and measured value is random. As an example, E_3 transitions have half-lives which are longer than the estimated values by a factor ranging from 10 to 10^6 and a mean value of 10^3 might be taken for this factor.

There are very few known M2's, so that one cannot say how our half-life compares with other known values in general, but it is consistent with the known ones and the 5×10^3 is not an unusually large value. Therefore, we can say that the assignment of γ_1 as an M2 is consistent with the Weisskopf estimates.

In conclusion one can say that Case 1 shows that γ_1 fits the experimental results to within experimental error as an M2, and γ_2 can have any multipolarity less than or equal to 2.

Case 2

It is assumed in this case that γ_2 is the isomeric transition. The Weisskopf estimates show that if the first transition is γ_2, it must be E3 or M3. The conversion coefficients for these multipolarities are:

TABLE IV

Multipolarity	E3	M3
Total	0.038	0.265
K	0.025	0.20

It can be seen that the maximum total conversion coefficient is 0.265 and therefore the maximum intensity which the 707 Kev transition can have would be 126. This would not change the assignment of γ_1 as an M2 since the accuracy of its intensity is not well enough known to distinguish between any of the cases. However, if we consider that γ_2 is an M3 then the intensity of γ_1 would be:

$$I_1 (1 + \alpha_1) = I_2 (1 + \alpha_2)$$

$$I_1 \times 17 = 100 \times 1.265$$

$$I_1 = 7.4$$

Therefore, the X-ray intensity would be

$$I_1 \alpha_K + I_2 \alpha_K = I_{K\ X\text{-ray}}$$

$$7.4 \times 10 + 100 \times 0.20 = I_{KX\text{-ray}}$$

$$I_{K\ X\text{-ray}} \doteq 100$$

This is much higher than the measured intensity and therefore we can remove M3 as a possibility. However, the possibility of the transition being an E3 is not eliminated by any of these considerations.

Therefore, the assignment of this transition as γ_2 being an E3 followed by γ_1 assigned as M2 is consistent with all the experimental information available. Nuclear structure systematics can be used to decide which of the two cases is more likely.

Discussion

We now have two alternatives (γ_1(M2) followed by γ_2, and γ_2(E3) followed by γ_1(M2)) from which to choose. Comparison with the known decay scheme of Pb^{203} strongly favours the first alternative. Pb^{203} and Po^{205} each have 121 neutrons (five vacancies in the closed shell at 126.) They differ in that Pb^{203} has 82 protons while Po^{205} has 84 (two outside the closed shell). The

two extra protons pair off and the ground state, which is determined mainly by the vacancies in the neutron shell, should be the same for both nuclei. The level scheme for Pb^{203} and the proposed scheme for Po^{205} are shown in the diagram.

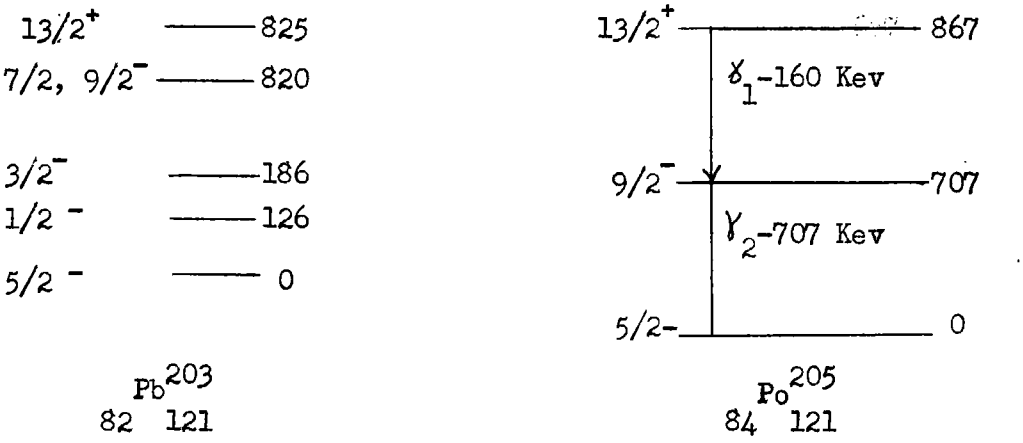

The lead has as its main feature the $5/2^-$ ground state and the six second isomeric state of $13/2^+$. This level is explained on the basis of the shell model and we would expect it in all the neutron deficient isotopes close to 126 neutrons. It is found systematically in the lead isotopes; therefore it should be expected in the similar polonium isotopes. It is quite reasonable to assume that it is causing the isomeric transition that we see, and that the decay in Po^{205} starts at the $13/2^+$ level and ends at the $5/2_-$ level. Since all the levels lying below the $13/2^+$ level should be of negative parity, we can reasonably expect only one change in parity.

Thus the shell model allows the following predictions:

1. The ground state is $5/2_-$.
2. The $13/2^+$ state exists.

3. The states of lower energy should have negative parity.

These considerations have been used along with the known presence of the 9/2− state in lead isomers to assign the decay scheme under Case 1.

Case 2 does not fit this picture very well since it requires two changes in parity and a total spin change of five. The shell model would predict only one change in parity and the only high spin state would be the $13/2^+$ level. Other high levels might be possible but it would usually require higher energies than are available.

It is also possible to get the high spin change by postulating that the ground state is 1/2−. But this does not allow us a way out from the double parity change.

Therefore, the previously assigned decay scheme fits with the known facts of shell structure and presents no unreasonable features. Although it needs more information to assign it unequivocally, it seems completely consistent with theory and experiment.

(b) Po^{207m_1}

1. Experiments

The first new isomer discovered was produced by protons on bismuth. The decay is shown in Fig. 16. The mean value of eight determinations is 47 ± 3 μsec. There is some difficulty in subtracting background and this may add a systematic error to these results.

The X-rays were very strong and a critical absorber experiment was done. The absorbers, their thicknesses and K-edge energies are:

TABLE V

Material	Z	Thickness	K-edge Energy
		gms/cm^2	Kev
Ta	73	0.234	67.48
W	74	0.252	69.50
Re	75	0.23	71.662
Os	76	0.23	73.86
Ir	77	0.23	76.097
Pt	78	0.228	78.374
Au	79	0.221	80.713
HgO	80	0.23(Hg)	83.106

These absorbers are all sandwiched between similar pieces of lucite and these pieces are then mounted in a lucite holder. The results of the experiment are shown in Fig. 17.

The K X-rays of Po and their energies are:

TABLE VI

Type	Energy	Intensity
	Kev	Arb. Units
α_1	79.296	2
α_2	76.868	1
β_1	89.809	0.6
β_2	92.386	0.14

FIG. 16

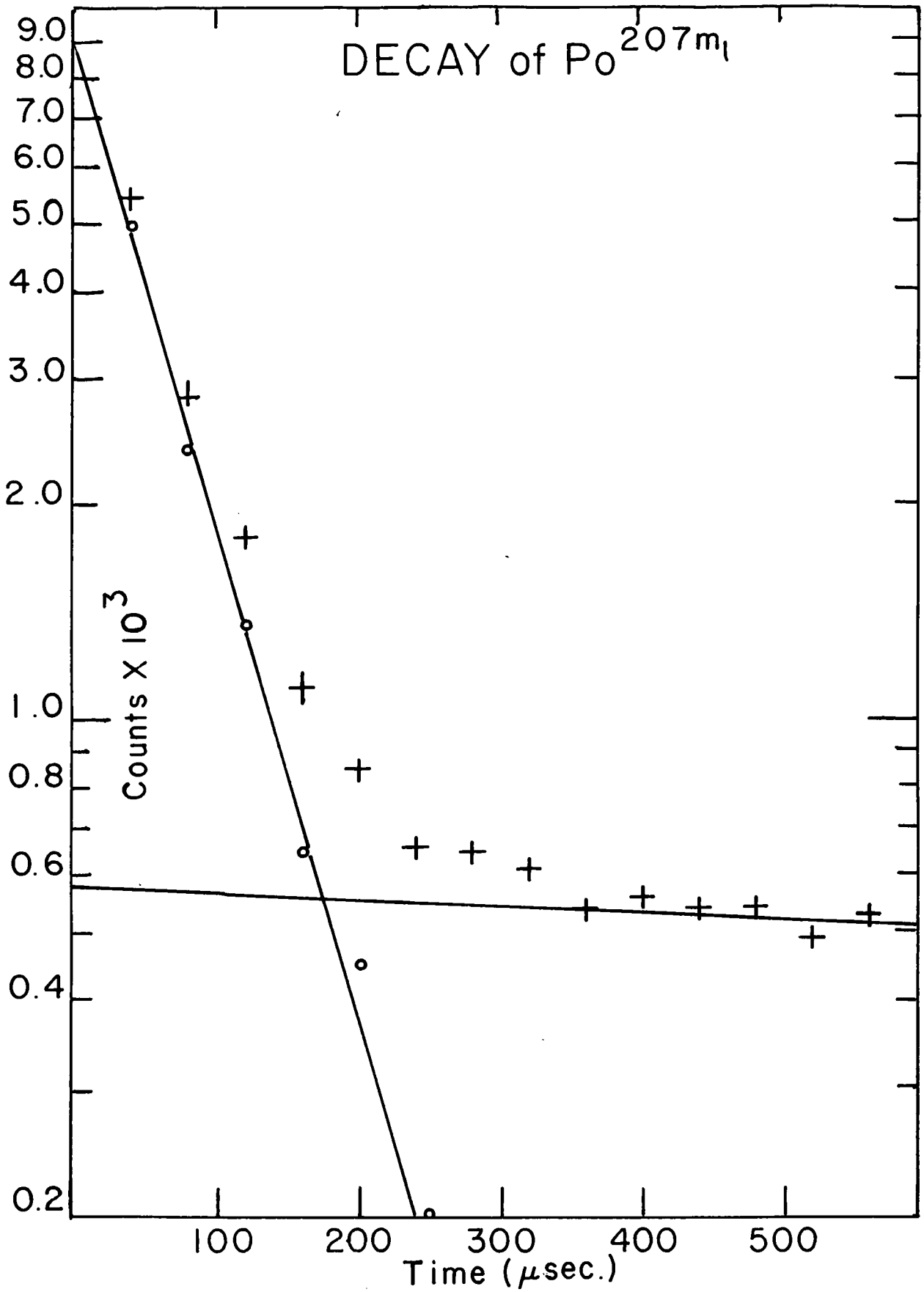
DECAY of Po^{207m_1}
9.0
8.0
7.0
6.0
5.0
4.0
3.0
2.0
1.0
0.8
0.6
0.4
0.2
Counts X 10^3
100
200
300
400
500
Time (μsec.)

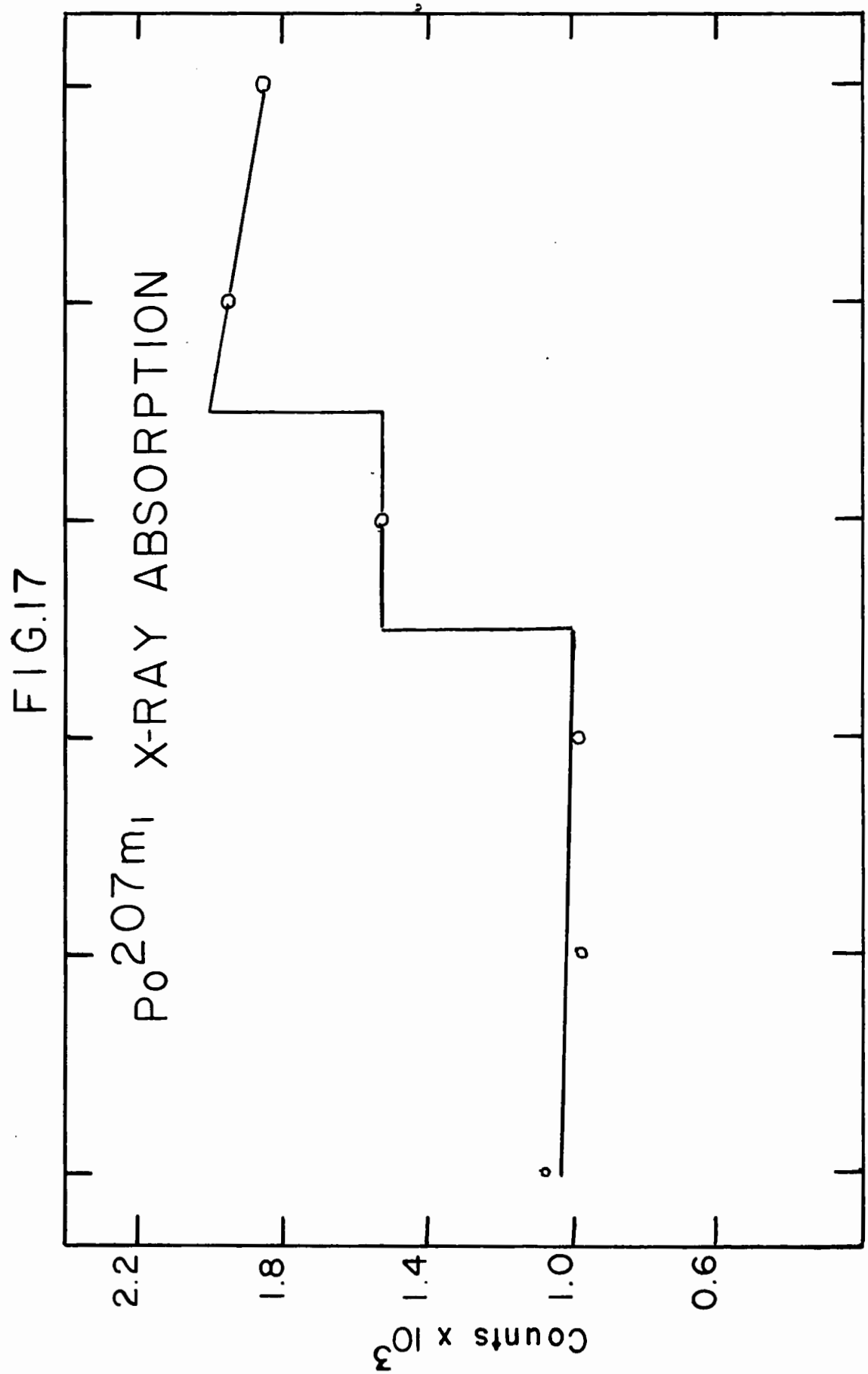
FIG.17
$Po^{207}m_1$ X-RAY ABSORPTION
Counts x 10^3
2.2
1.8
1.4
1.0
0.6
Re
Os
Ir
Pt
Au
Hg
Absorber

A comparison of the binding energies of the K shell electrons of the absorbers and the emission spectrum of Po leads to the conclusion that the emission spectrum of Po would be absorbed by all the absorbers up to Ir. At Pt, the $K\alpha_2$ line of Po would be transmitted and at Au the $K\alpha_1$ line would be passed. There would then be only a slight increase in the absorption as the remaining absorbers were interposed.

Comparing this expectation with Fig. 17, we see that the first increase in X-ray intensity occurs at platinum and the second at gold. Consequently, the X-rays are those of polonium.

The relative height of these steps is not in a proportion to account for the known intensities of the lines. This is explained as being due to the excitation of the characteristic X-ray radiation of the absorber by the primary radiation. This secondary radiation is not resolved from the primary radiation by the NaI(Tl) drystal. Since the absorber has nearly 2π geometry relative to the crystal, something less than half of these secondary X-rays are detected. Further, the effective thickness of the absorber will be increased due to the angle at which the X-rays may traverse the absorber and still be detected in the crystal, thus making it difficult to predict the effective thickness of the absorber.

Yield Curve

An attempt was made to measure the yield as a function of bombarding energy. This was done at three energies, the results of which are shown in Table VII.

TABLE VII

E_p	Counts/burst
Mev	
40	7.4×10^{-2}
30	16.2×10^{-2}
20	4.4×10^{-2}

This is a fairly clear indication that it is a $Bi(p, 3n)Po^{207}$ reaction and the nucleus is assigned as Po^{207}. It is to be noted that the actual increase in yield in going from 40 to 30 Mev is greater than is shown by these figures, since the protons striking the target are reduced in number as well as in energy because of the increase in scattering which accompanies the increase in beam absorber thickness. It is further to be noted that the yield would not drop nearly as much above 30 Mev if it were a (p, pxn) reaction.

The Energy Spectrum

The energy spectrum of $207m_1$, as well as that of $207m_2$ which will be discussed later, is shown in Fig. 18. This spectrum is taken with a delay of 25 μsec and a gate length on the phototube of 100 μsec. The target is bismuth foil 0.021" thick. The principal features of the $207m_1$ spectrum are the strong X-rays, the γ-rays at 315 $\pm$ 10 Kev and at 820 $\pm$ 15 Kev.

A check was made to see if all the lines had the same half-life. The experiment was done by using a constant gate on the phototube and varying its delay relative to the arrival of the proton burst. The phototube gate was delayed for 20, 100 and

FIG. 18

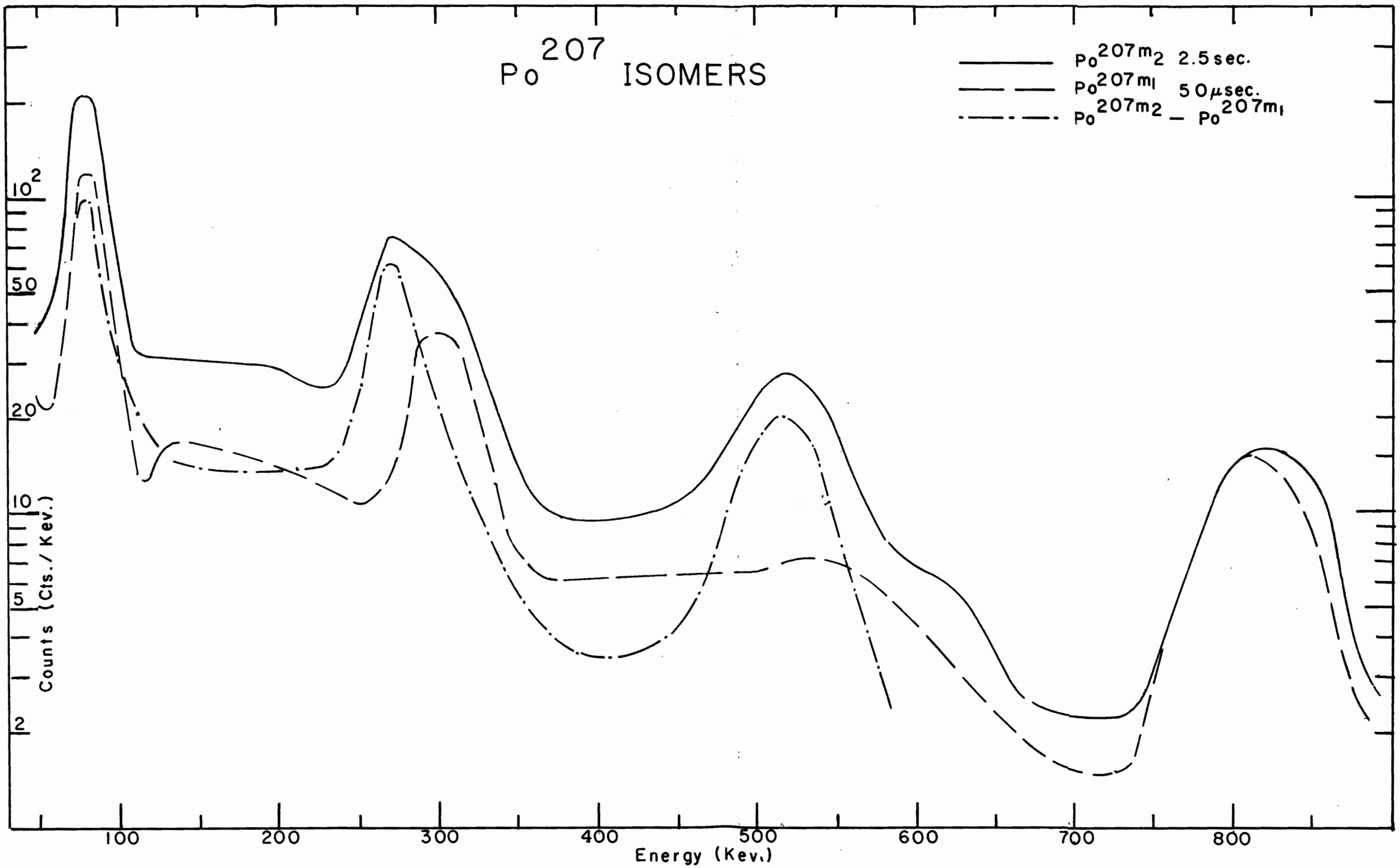
Po 207 ISOMERS
Po207m2 2.5 sec.
Po207m1 50 μsec.
Po207m2 – Po207m1
Counts (Cts./Kev.)
10²
50
20
10
5
2
100
200
300
400
500
600
700
800
Energy (Kev.)

500 μsec. after the arrival of the protons and then opened for 100 μsec. The results are shown in Table VIII.

TABLE VIII

Delay	I(315)/I(820)	I X-ray/I(820)
μsec		
20	1.5	3.61
100	1.4	3.81

This table shows that the relative intensity of the γ-rays and X-rays were fairly consistent over the delay range 20 to 100 μsec. The 500 μsec delay still shows some evidence of this decay. This is surprising but will be accounted for when we discuss the second isomer discovered in this nucleus.

The next problem was to measure the relative intensities of the components of the decay. To do this the photopeaks of the γ-rays were fitted to gaussian curves (see appendix 2) in order to obtain the proper shape of the background and also to ensure that the peaks are all single. The results are shown in Table IX.

TABLE IX

E	Kev	820	315	X-ray
Counts		2221	2894	4974
NaI Effic.		3.8×10^{-3}	1.1×10^{-2}	3.8×10^{-2}
Rel. Int.		100	44.9	22.4

Target self-absorption is not taken into account in this table. Only the X-rays are affected to an important degree. To measure the X-ray absorption, the X-ray intensity was plotted relative to the 820 Kev γ-ray intensity as a function of target thickness and the result extrapolated to zero thickness. This involves the assumption that a linear extrapolation is adequate.

In order to check this assumption, an attempt was made to calculate the magnitude of the effect from the known absorption coefficients of the material. If I_x is the X-ray intensity per unit thickness and "a" is the target thickness, the number of X-rays which escape from the target from an element dx at a depth x in the target is

$$dI = I_x dx\, e^{-ux}$$

This is really the number of those which emerge, having started in the detector direction. A straight forward integration of this formula over the target thickness yields the result that the measured intensity would be

$$I = \frac{Ix}{u}(1 - e^{-ua})$$

This simple approach ignores the fact that the target is at 45° to the axis of the counter. This effect is taken into account by multiplying a by $\sqrt{2}$. Another effect which is ignored is the variation of the solid angle which the counter subtends at each point in the target. The plot of this formula with the thickness equal to $\sqrt{2}$ a is shown in Fig. 19 along with the experimental X-ray intensity. The two compare very favourably and this shows that the extrapolation of the straight line is within experimental

FIG.19

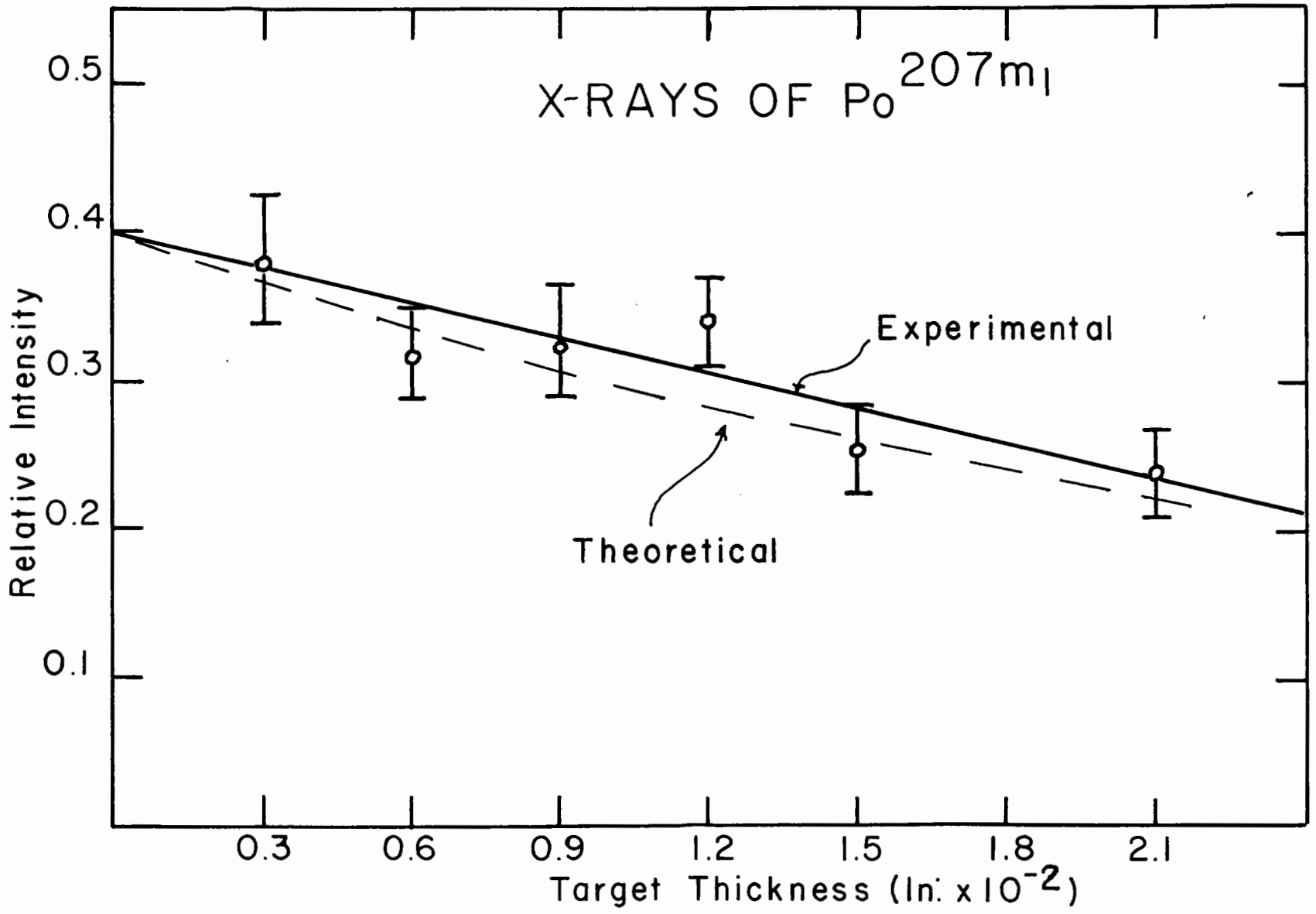
X-RAYS OF Po 207m1
Relative Intensity
0.5
0.4
0.3
0.2
0.1
Experimental
Theoretical
0.3
0.6
0.9
1.2
1.5
1.8
2.1
Target Thickness (In. x 10-2)

error over the region of target thickness used in this experiment.

The target thickness used in the relative intensity measurement was 0.021" and therefore the X-ray intensity is increased by a factor 0.4/0.24, which leads to an intensity of 37.3. This is further corrected for Auger loss which increases the X-ray intensity to 39.

2. Analysis

For the purpose of this analysis the γ-rays shall be designated as follows:

γ_1 ..... 820 Kev

γ_2 ..... 315 Kev

γ_3 ..... X-rays

The following possibilities exist on the assumption that there are no unobserved γ-rays and that the two γ-rays are in cascade.

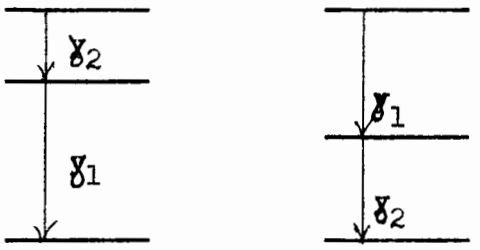

Case 1 Case 2

CASE 1

This assumes that γ_2 is the isomeric transition followed by γ_1. This narrows the possibilities considerably since the total intensity for the 315 Kev transition must equal that of the 820 Kev transition, that is

$$I_1(1+\alpha_1) = I_2(1+\alpha_2)$$

Unless otherwise stated, alpha will be the total conversion coefficient. Since for this case α_1 is not the isomeric transition its conversion coefficient should be small and it will be ignored. Therefore:

$$\frac{I_1}{I_2} = 1+\alpha_2$$

$$\alpha_2 = \frac{100}{449} - 1$$

$$= 1.22$$

The calculated total conversion coefficients from Rose's tables for a 315 Kev γ-ray are:

TABLE X

Multi-polarity	β_1	β_2	β_3	β_4	α_1	α_2	α_3	α_4
Total	0.44	1.55	5.9	16.5	0.026	0.1	0.6	3.3
K	.35	1.12	3.05	7.5	0.22	0.06	.16	.42

It is seen that the only reasonable value is 1.55. Therefore it is assumed that this is an M2 radiation. Since the inherent error in the measurements is large it seems more reasonable to use the calculated values as a basis for further comparison. Using the calculated value of the conversion coefficients, the relative intensities of γ_2 and γ_1 would be 39 and 100 respectively.

From this the X-ray intensity would be

$$I_2 \alpha_{k2} = 39 \times 1.1 = 43$$

This is within the experimental value of the X-ray intensity.

The next point of comparison is the Weisskopf estimates. The experimental half-life for γ-ray emission on the above assumption is 120 μsec. The Weisskopf estimates give the value of 0.7×10^{-7} sec. Thus the experimental value exceeds the calculated value by a factor of 1.7×10^{3}. Since this is an M2 radiation our previous remarks about the Weisskopf estimates are applicable, and one concludes that the M2 assignment is possible.

Case 2

Here we assume that γ_1 is the isomer, but cannot assume that α_2 is negligible. However the Weisskopf estimates can give an indication of the multipolarity of the γ-ray and hence the possible conversion coefficients. For an 820 Kev γ-ray the only reasonable multipolarities from the Weisskopf estimates are either E3 or M3. The conversion coefficients for these are:

TABLE XI

Multipolarity	E3	M3
α_T	2.25×10^{-2}	1.5×10^{-1}
α_K	1.7×10^{-2}	1.15×10^{-1}

If γ_1 is E3, conversion of the isomer is again negligible and analysis proceeds as for Case 1. That is to say, we would

have γ_1 E3 followed by γ_2 M2.

The other possibility is for γ_1 to be M3. In that case

$$\frac{I_1(1 + \alpha_1)}{I_2(1 + \alpha_2)} = 1$$

$$\frac{100(1 + 0.15)}{45.0(1 + \alpha_2)} = 1$$

$$\alpha_2 = 1.60$$

This is in agreement with the total conversion coefficients for an M2. Using these values, the X-ray intensity is

$$100 \times 0.11 + 45 \times 1.1 = 60$$

This value of the X-ray intensity is 50% greater than the measured value and therefore we discard it as a possibility.

The case for an E3 followed by an M2 fits well with experimental evidence but seems less probable on theoretical grounds because both γ-rays would have comparable half-lives. Also, it would require two changes of parity and this would be inconsistent with a shell model picture of nuclear structure in this region.

(c) Po^{207m_2} 1. Experiments

While bombarding Bi^{209} with protons at 30 Mev, two very strong γ-rays appeared at all time intervals beyond 1 msec. No decay was observable, however, at even the longest setting of the time interval of 40 msec per channel. It was decided to look at

the energy spectrum in the kicksorter immediately after a two-second bombardment and see if there was an observable decay. A short decay was obvious and a second new isomer was discovered.

Since the half-life was longer than the apparatus would normally handle, some modifications were necessary to study this isomer. The beam switching tubes, instead of being driven by the time marker generator, were driven by the scale of 64, which was itself driven from the 60 cycle frequency of the mains. It was manually controlled, as were also the cyclotron and phototube. Poor reproducibility was introduced by this method of actuating the various components. The half-life was found to be 2.5 ± 1 sec. A typical half-life curve is shown in Fig. 20. The large background is due to an interfering activity believed to be in the iron of the castle. This background and the manual control are responsible for low accuracy in this measurement.

The Critical Absorber Experiment

The K X-rays in the previous spectrum were very strong and a critical absorber experiment was done. This experiment was similar to that for the Po^{207m1} in all its details except for the control of the cyclotron. The beam was turned on at full cyclotron repetition rate until the beam monitor read full scale and the cyclotron beam was then switched off. Approximately one second later the kicksorter was turned on for 10 seconds. This procedure was repeated for each absorber. The number of counts in each channel under the X-ray peak was measured and normalized to the same beam strength. The results are plotted in Fig. 21.

FIG.20

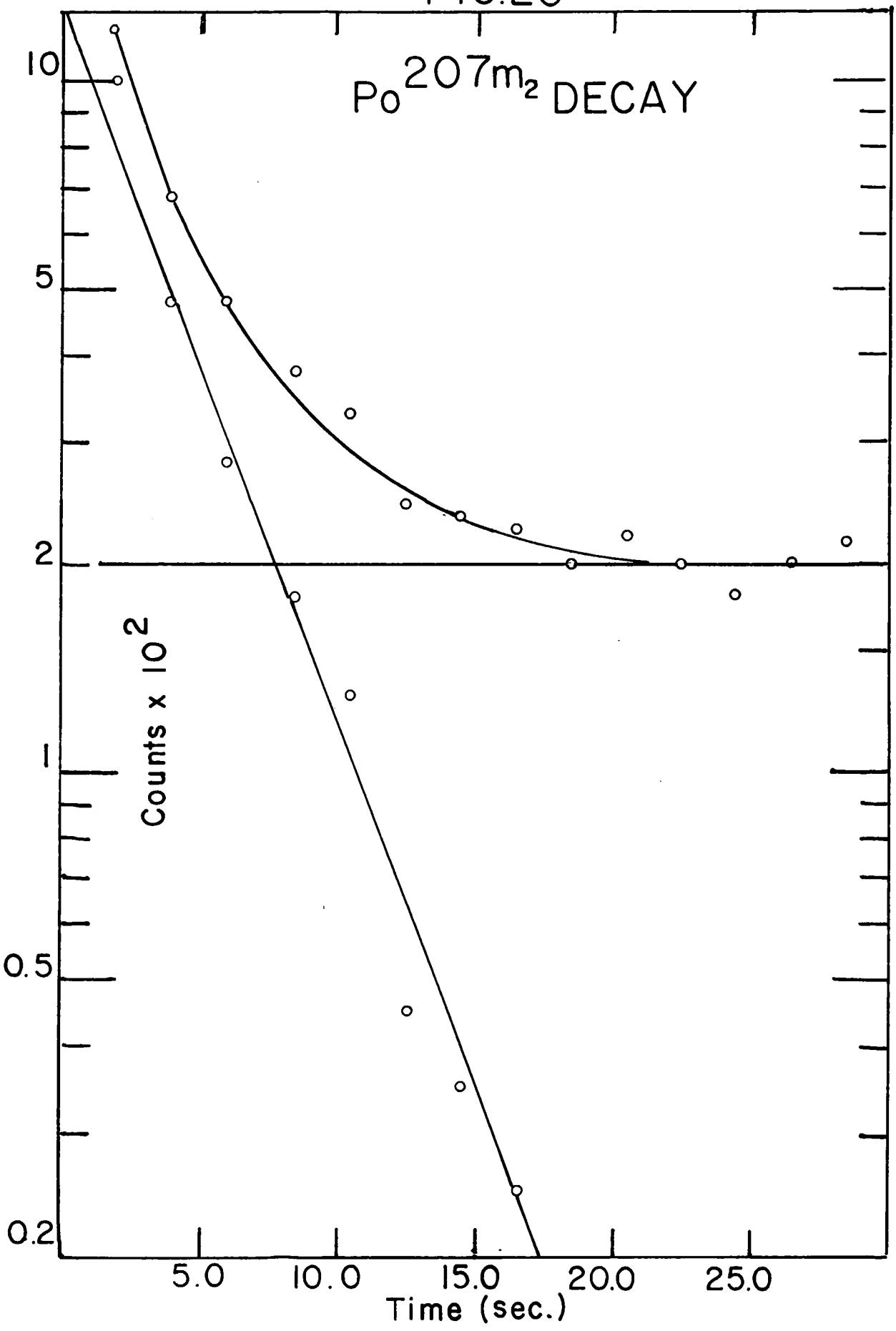
Po 207m2 DECAY
10
5
2
1
0.5
0.2
Counts x 10^2
5.0
10.0
15.0
20.0
25.0
Time (sec.)

The indicated spread in the points is that of statistical fluctuations only. Uncertainty in the timing would tend to increase these errors. One can conclude, however, that these X-rays are from Po.

The Energy Spectrum

This spectrum, as shown in Fig. 18, characterized by two γ-rays, one at 820 Kev, one at 284 Kev and an X-ray peak due to polonium as well. An attempt was made to fit both γ-rays to a gaussian curve. The 820 Kev peak was found to fit quite closely but the 284 Kev peak did not fit. The latter was examined more closely and found to be in reality an unresolved double peak. It was fitted as nearly as possible to two peaks and the energies roughly estimated as 310 Kev and 260 Kev.

This spectrum was next compared to that of the 50 μsec isomer in Po^{207m1}. It was postulated that the 820 Kev γ-ray and the 315 Kev γ-ray of this isomer must be the same as the 820 Kev and 310 Kev γ-rays of the 2.5 sec isomer, and that the 260 Kev γ-ray arises from a transition between a new 2.5 sec isomer and the previously studied 50 μsec isomer. With this in mind the two spectra were normalized to one another and subtracted. The results of this procedure, shown in Fig. 18, confirm our postulate. We assign the energies of these γ-rays as:

260 ± 20 Kev

315 ± 10 Kev

820 ± 15 Kev

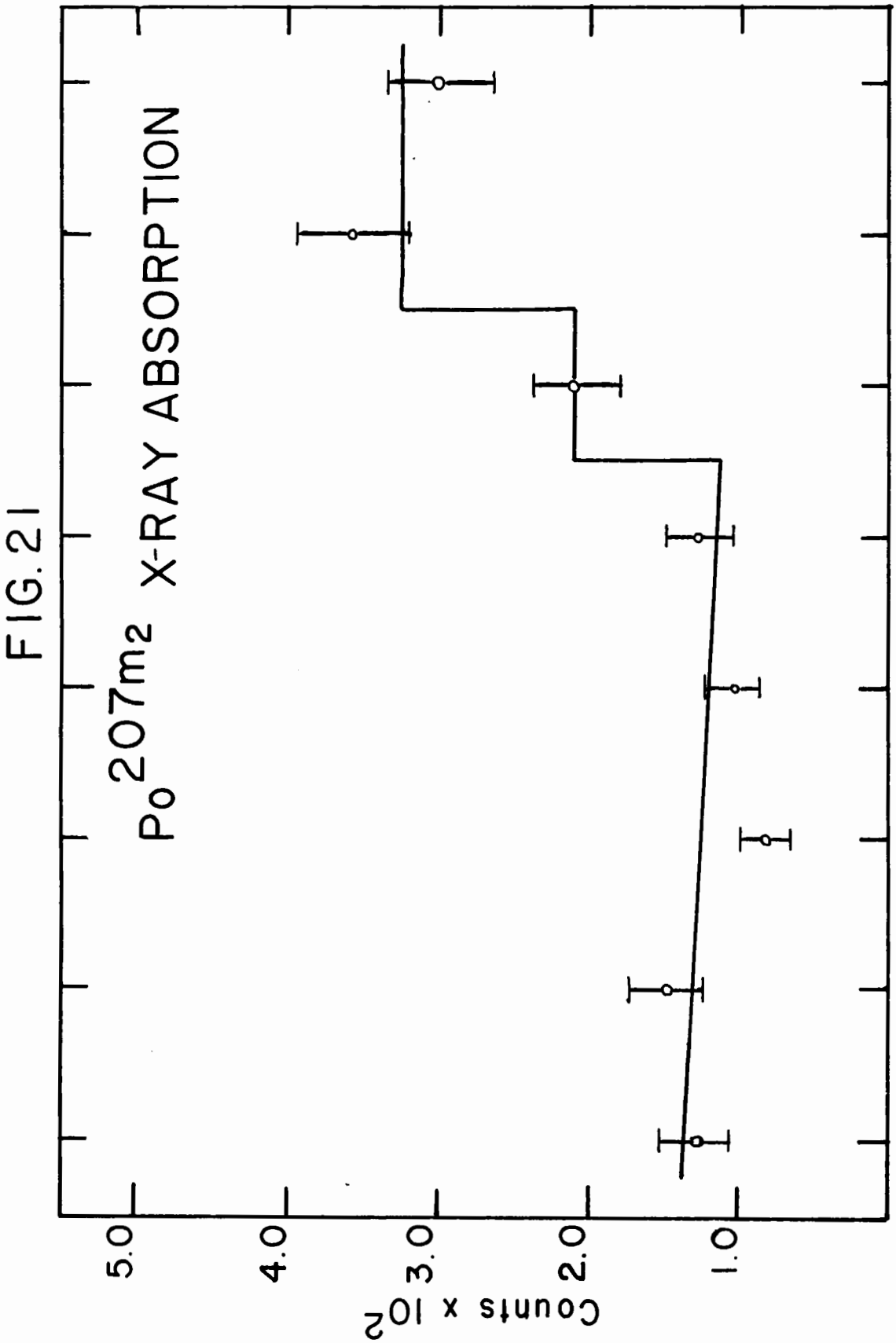
FIG. 21
Po^{207m_2} X-RAY ABSORPTION
Counts x 10^2
5.0
4.0
3.0
2.0
1.0
Ta
W
Re
Os
Ir
Pt
Au
Hg
Absorber

The relative intensities of the 260 Kev γ-ray and the 315 Kev γ-ray were difficult to measure. Therefore it was decided to measure their combined intensity and subtract the intensity of the 315 Kev γ-ray as calculated from the previous analysis of the 50 μsec isomer. The measured intensities of the 2.5 sec isomer are given in Table XII

TABLE XII

E	Kev	820	315 + 260	X-ray
Intensity		100	80.5	60

These intensities are corrected for counter efficiency, target thickness and in the case of the X-rays, for Auger effect.

2. Analysis

To analyse the above results we must decide what intensities to use for the 50 μsec activity γ-rays when this is subtracted from the 2.5 sec activity. In the analysis of the 50 μsec activity it was decided that the 310 Kev γ-ray was most likely to be an M2. On the assumption that it was an M2 its intensity relative to the 820 Kev γ-ray was then calculated and this is the value which is most reasonable to use in the subtraction. On this basis, the relative intensities are shown in Table XIII.

TABLE XIII

E	Kev	820	310	X-ray
Intensity		100	39	44

Subtraction of these leads to an intensity of 41.5 for the 260 Kev γ-ray and 16 for the associated X-rays. Therefore, the total conversion coefficient of the 260 Kev γ-ray is

$$41.5\ (1 + \alpha) = 100$$

$$\alpha = 1.41$$

The calculated conversion coefficients for the 260 Kev γ-rays are

TABLE XIV

Multipole	E2	E3	E4	M1	M2	M3	M4
α	.19	1.3	9.2	.74	2.9	44	105
α_K		0.25					

Of these the only reasonable one is E3 with a conversion coefficient of 1.3. Therefore, the calculated intensity would be 43.5. Because of the errors in the measured intensities it is reasonable to use this calculated value of the intensity to determine the X-ray intensity. This would be

$$I \times \alpha_K = 43.5 \times 0.245$$

$$= 10.6$$

This value of 10.6 is to be compared with the experimental value of 16. This agreement is poor until we consider that the total calculated value 44 + 10.6 = 54.6, which is to be compared with an experimental value of 59. This is an error of 10%, which is reasonable agreement.

The final consideration is the Weisskopf estimates. The measured half-life is 2.5 sec. The γ-ray half-life will be

$$T_{\frac{1}{2}r} = T_{\frac{1}{2}}(1 + \alpha)$$

$$= 2.5 \times 2.3$$

$$= 5.75 \text{ sec.}$$

The Weisskopf estimates for this transition would be 10^{-3}. Thus the measured half-life is about 6000 times the Weisskopf estimates, as is commonly the case for E3 transitions.

Discussion

In order to fit these results into the Po^{207} level scheme we must turn to the comparable isotope Pb^{205}.

The level scheme is

$13/2^+$ ———— 1.014

$9/2-$ ———— 0.988

$7/2-$ ———— 0.703

$3/2-$ ———— 0.260

$5/2-$ ———— 0

It is seen that the state which causes isomerism is the $13/2^+$ level and that it decays to the $9/2-$ level by M2 radiation. Also the ground state is $5/2-$. This scheme should be the same at least qualitatively for Po^{207}, which has the same number of neutrons but two extra protons outside the closed shell of 82 in lead. The protons will probably shift the levels at least slightly in energy and may produce some new states, but leave the old states from the excitation of the neutron hole still there. The fact that the ground state of Po^{207} is suspected to be $5/2-$ indicates

that it has not been changed by the addition of the two protons and this adds some weight to the arguments of similarity.

On comparison of these levels in Pb^{205} with the ones in Po^{207}, it seems that the $13/2^+$ level is the 50 μsec isomer and that it decays by M2 radiation to a 9/2- level which then decays by E2 radiation to the ground state. The 2.5 sec isomer is more difficult to understand. It is, however, probably due to the excitation of the two extra protons in combination with the neutron hole which produces the high spin state. This would have to be a 19/2- state. Therefore, the decay scheme of these two isomers is tentatively assigned as follows:

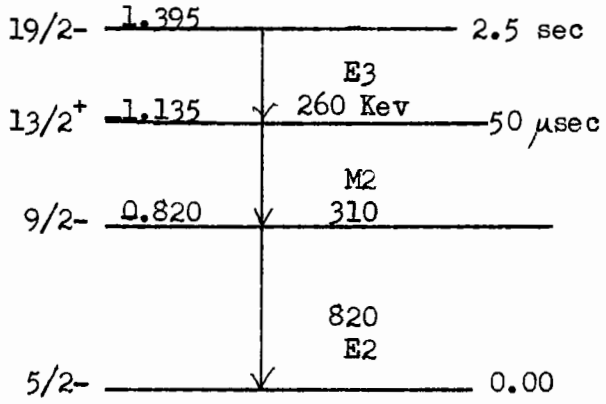

This scheme seems to provide the best agreement with the available information.

Level Systematics

The levels in neutron deficient odd mass number lead isotopes are known to have a relatively smooth variation as neutrons are removed. The variation of the $13/2^+$ level was shown to be linear when measured relative to the 5/2 level by Stokendahl et al[33,34]. Also this level in mercury shows the same trend among the known levels. This smooth variation has been handled theoretically by Kisslinger and Sorensen[35] and has been shown to apply to many of the levels.

It is reasonable to assume that the same general variation in the levels of lead should carry over to polonium. A comparison of the $13/2^+$ and 9/2- levels in lead with those assigned by these experiments to polonium is shown in Fig. 21A. The points of similarity are: a) The slope of both curves have the same sign as those in lead. b) The slope of the 9/2- levels are changing relative to the $13/2^+$ in the same manner in both elements, although the magnitude of the change is different. c) The magnitudes of the energy of the $13/2^+$ levels in lead and polonium are roughly the same, being within about 100 Kev. This last statement is corroborated by the known $13/2^+$ levels in mercury which show a difference in the opposite direction of roughly the same amount.

There is good corroboration in the systematics of the levels in this region for the assignment of the levels found in polonium. On the basis of these systematics it would seem possible to predict the energy of other $13/2^+$ states in polonium.

A simple extrapolation of the two points should give an idea of the expected energy. A search was made in the time range available with this apparatus and over an energy range from 10 - 90 Mev. No measurable decays were found. A further search in other time ranges might be undertaken with more success by other means.

CONCLUSIONS

The operating current of the cyclotron magnet was increased and hence more of the internal beam was extracted. The focusing of the exit channel was changed by the higher magnet current. Therefore the channel was reshimmed. The steering magnet was also rewound. A final external beam of 1.31×10^{-10} amps was obtained with an energy of 90.6 Mev and a full width at half maximum of 1.2 Mev.

The background was reduced by the construction of a new castle. This castle was made of iron in the form of a hollow cube. The wall thickness of the cube was 5" and the inside dimension was 18". The background was reduced to 338 cps at 50 μsec after the beam passed for all γ-rays above 50 Kev.

An electronic switching mechanism was built which sorted the pulses according to their arrival after the exciting burst of protons. The Burroughs Beam Switching Tube was used to turn on series of integrators consecutively. All the pulses which arrived during the "on" time of a particular integrator were stored in that integrator. Thus any decays were displayed by the integrators.

With this apparatus two new isomers were discovered in Po^{207} and more information was found on the decay of a known isomer in Po^{205}. A half-life of 47 ± 3 μsec was found for the first isomer. It was characterized by two γ-rays, one of 310 Kev and the other of 820 Kev. The multipolarities were found from

the relative intensities of the γ-rays and X-rays and from the shell model to be M2 and E2 respectively. The isomerism was caused by the decay of the $13/2^+$ state to a 9/2- state, followed by a decay to the 5/2- ground state. The half-life of the second isomeric state in Po^{207} was found to be 2.5 ± 1 sec. It showed only one γ-ray of 260 Kev and an estimated multipolarity of E3. It decayed to the $13/2^+$ state already mentioned.

A new γ-ray was found in the decay of the 644 μsec isomer in Po^{205}. It had an energy of 160 Kev. The decay scheme was found to be 160 Kev (M2) followed by 707 Kev (E2). This was assigned to the decay of the $13/2^+$ level in polonium to a 9/2- level and then to the 5/2- ground state on the basis of the relative intensities of the γ-rays and the X-rays in conjunction with the level systematics and the shell model of nuclear structure.

A survey of the neutron deficient polonium isotopes was made by bombarding bismuth with protons of energies from 90 to 10 Mev and in the time range from 20 μsec to 0.1 sec. No measurable activities were observed in this range, other than the ones already mentioned.

In conclusion, the two new isomers were discovered by bombarding only one element, and considerable information on a third. This seems to indicate that there are undiscovered isomers in this range and that more work is necessary in this range of half-lives.

FIG. 21A

LEVEL SYSTEMATICS

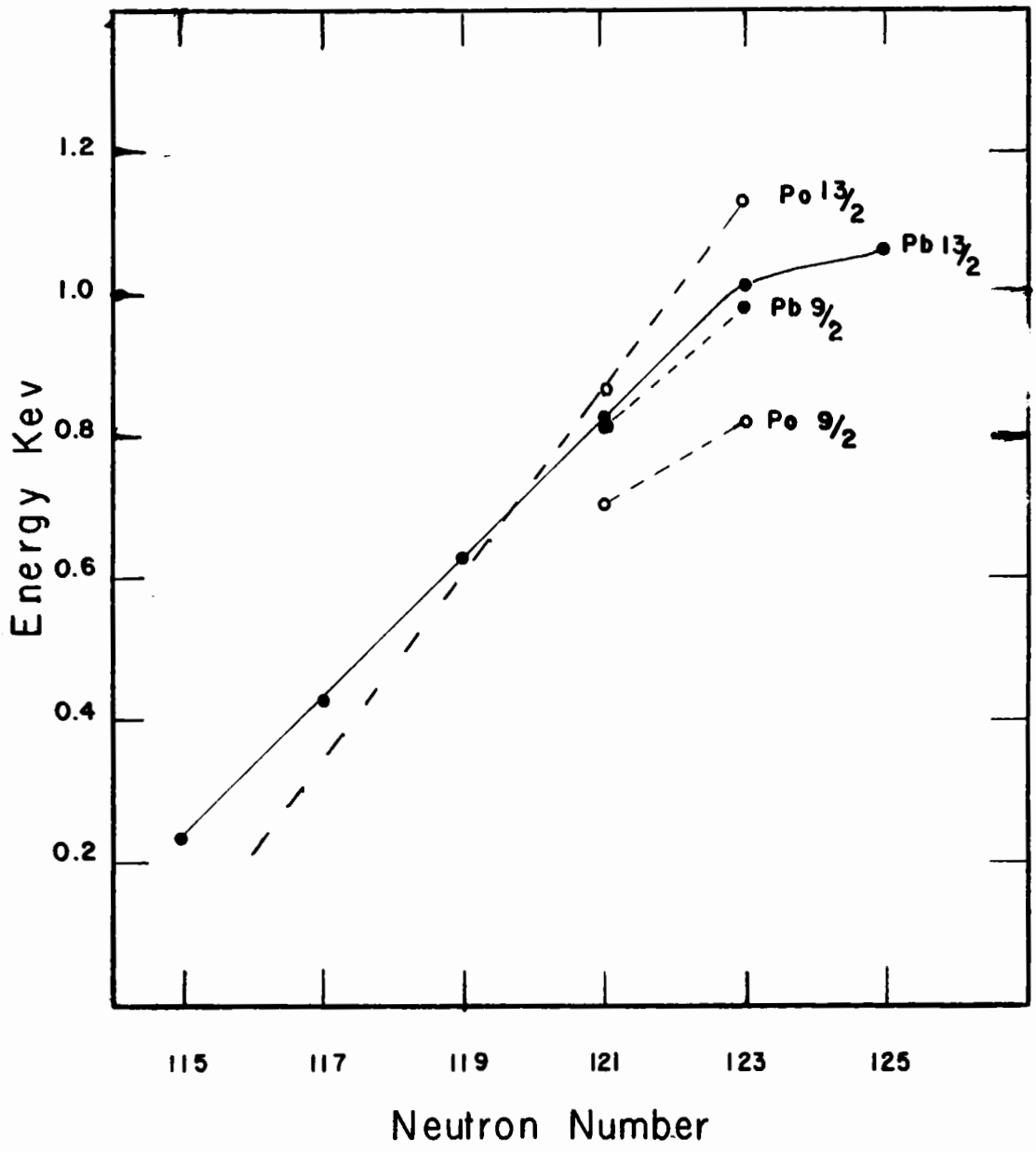

BIBLIOGRAPHY

1. E. Arbman. Nucl. Phys. 3, 625.

2. D.E. Alburger, G. Friedlander, Phys. Rev. 81, 523.

3.) S. DeBenedetti, U. Farinelli, F. Ferrero, R. Halvano, G. Pelli,
4.) C. Tribuno, Nuovo Cincento 6, 682.

5. E.M. Bowey, Nucl. Phys. 3, 553.

6. R.B. Duffield, S.H. Vegors Jr., Phys. Rev. 112, #5, 58.

7. K.N. Geller, E.G. Muirhead, J. Halpern. Bull. Am. Phys. Soc. 4 #1, 56.

8. V.R. Glagolev, O.M. Kovrizhnykh, Yu.V. Makarov, P.A. Yampol'skii, J. Exptl. Phys (USSR) 36, 1046-1051 (April '59).

9. M. Goldhaber, A.W. Sunyar. Beta and Gamma Ray Spectroscopy. Kai Seigbahn North-Holland Publishing Co.

10. C.L. Hammer, M.G. Stewart. Phys. Rev. 106, 1001 (57)

11. C.L. Hammer, M.G. Stewart. Bull. Am. Phys. Soc. 1, #4, 206 R2 (56).

12. Leipunskii, Morazov, Makarov, Yampol'skii. J. Exptl Theoret. Phys. (USSR) 32, 393 (1957) Soviet Phys. JETP 5, 305, 57.

13. Leipunskii, Miller, Morozov, Mampol'skii. Dokl. Akad, Nank. SSSR 108, 935 (1956). Soviet Phys. Dokl 1, 505 (57).

14. W.T. Link. Ph.D. Thesis, McGill Univeristy 1957.

15. C.L. McGinnis. Phys. Rev. 109, 888, 58; 98, 1172A (55)

16. D.W. Martin, S.B. Burson, J.M. Cork. Bull. Am. Phys. Soc. 1, #8, 389 M_3 1956 UCRL 3538.

17. J.W. Mihelich, B. Harmatz, J.H. Handley. Bull. Am. Phys. Soc. 3, #7, 358 A6 (58)

18. P.D. Miller, W.M. Good, J.M. Gibbon, J.H. Neiler; Bull. Am. Phys. Soc. 4 #1, 42 R1

19. M.D. Petroff. Bull. Am. Phys. Soc. 1 #8, 389 M_3 1956 URCL 3538 (1956)

20. J.M. Ponce de Leon, C. Sanchez del Rio; Annales real soc espan fis y quin. 52 A 137.

21. A.W. Schardt, A. Goodman. Bull. Am. Phys. Soc. 4 #1 56 VA 1 Oral Report.

22. Softky, S.D. Phys. Rev. 98, 736 (55).

23. P.A. Tove. Nuclear Instr. 1, 95.

24. C.C. Trail, C.H. Johnson. Phys. Rev. 91, 474 A.

25. S.H. Vegors Jr., P. Axel. Phys. Rev. 100, 1238 H (55).

26. S.H. Vegors Jrs., P. Axel, Phys. Rev. 101, 1067 (66)

27. S.H. Vegors Jr., R.B. Duffield. Bull. Am. Phys. Soc. 1 #4, 206 R1.

28. Yampol'skii, Leipunskii. Gen, and Tikhomirou. Isv. Akad, Nauk SSSR. Ser Fiz. 19, 338 (55).

29. R.D. Evans. The Atomic Nucleus. McGraw Hill.

30. I.E. Lindstrom, B. Crosemann. R.S.I. 30, #5 (59).

31. R.E. Bell, H.M. Skarsgard. Can. Jour. of Phys. 34, 745 (1956).

32. J.D. Jackson, Can. Jour. of Phys. 34, 767 (1956).

33. J.D. Stokendahl, J.A. McDonell, M. Schmorak and I. Bergstrom, Arkiv f. Fysik 11, 165.

34. R. Stokendahl. Arkiv f Fysik 17, 553.

35. L.S. Kisslinger, R.A. Sorensen. Det Kongelige, Danske Vedenskabernes Selskals Matematisk-fysiske meddelelser. (to be published).

36. I. Boekelheide. R.S.I. 31, 100 1, (1960).

APPENDIX I

ELECTRONICS

Further details of the electronic instrumentation outlined in the text are given in this appendix.

In Fig.22 the phase inverter and the first delay circuit are shown. The phase inverter adapts the positive output of the "Atomic Al" amplifier to the negative input of the integrators and also adds a fixed voltage or pedestal to each signal. This latter is necessary since the integrators have a fixed threshold below which no integration occurs. The unit employs a clipping circuit and an anode follower. The signal is clipped down to a fixed level set by the 100 K potentiometer, thus producing its own pedestal. The original signal goes directly to the input of the anode follower where it is added to the pedestal. The output of the anode follower goes to the eighteenth integrator where it is stored. The accumulation in the integrator is a measure of the number of protons hitting the target.

The second circuit is the first delay. It is a basic univibrator circuit with a delay variable from 50 μsec to one msec.

The Beam Switching Tube pulser unit is shown in Fig. 23. The input from the Time Marker Generator (TMG) is sent into a twin triode gate circuit. This circuit is used to gate only the 10 μsec pulses from the TMG. It was found necessary to do this because of difficulties affecting the oscillator of the TMG if gating was done internally. The other ranges of the TMG were gated internally

by a similar circuit placed after the 10 μsec output. This, of course, means that the oscillator is running in the TMG at all times and that there is an uncertainty in the starting time of the Beam Switching Tubes (BST) of 10 μsec. This was felt to be unimportant for the work done here.

The output from this gate is amplified and inverted and sent to two scales of two in series so that the TMG output time scale may be multiplied by either two or four. This was necessary since the TMG output was variable only by factors of ten. These outputs are then sent through a cathode follower to the BST driver, Fig. 24. After the last position of the BST is finished, a signal is sent to the reset univibrator (Fig. 23) which has an "on" time of 10 μsec. This reset univibrator puts the scales of two in the correct phase and also shuts off the TMG by flipping its gating scale of two. The TMG gating scale of two gives the signal which opens and shuts the two gates of the TMG. It receives its "on" signal from D1 (Fig. 22) and its "off" signal from the reset univibrator.

The TMG Gating Scale of 2 and the TMG Fast gate act as a unit to turn the TMG off and on. The TMG is normally held off. This is done by having the right hand grid of the fast gate bias above the other grid so that it is conducting. When the signal from D1 (Fig. 22) is sent to turn the TMG on, the TMG gating scale of 2 flips and the right hand anode, which is normally conducting, is shut off and the voltage rises. This is used to raise the left hand grid of the fast gate enough to cause it to conduct and allow the TMG pulses to pass. When the signal is sent from the BST

to turn the TMG off, the system returns to its rest position.

The BST driver and BST are shown in Fig. 24. The driver is a scale of two. The outputs from the plates are sent respectively to the even and odd grids of the two BST's, but first they are differentiated and the positive spike is clipped by the 6AL5 diode. The D.C. level of the grids is controlled by the 100K potentiometer. The pulse height of the grid signals is controlled by the potentiometer in the plates of the driver. The beam switching tubes circuits are copied from the manufacturer's specifications. The cathode follower (6C4) sends the output from the 18th position to the reset univibrator of Fig. 23.

In measuring half-lives that are shorter than 100 μsec it is often necessary to have the phototube gated for a time shorter than the time gate on the BST which is normally used to control the phototube. For these times a special univibrator was built with a variable delay from 20μsec to 300μsec. This is shown in Fig. 25. Also shown in Fig. 25 is a White cathode follower which is used to send the gating signal to the phototube from either the short gate or the TMG gating scale of two. It is D.C. coupled to allow for long times and has a switch that allows the phototube to be turned on and off manually.

Each position of the BST is used to activate its own integrator. This is done through an intermediate coincidence circuit which is shown as Input to Integrator N. The left grid of the 6J6 is tied to one spade of a BST. When that spade is turned off the grid is at ground potential and all the current is sent through the left side. When the spade is turned on the grid is dropped

approximately 20 V, but not enough to change the conduction. But now if a pulse comes from the Single Channel Analyzer it is enough to shift the current from the left to the right side and a pulse is sent to the integrator.

In Fig. 26 the Cyclotron gating scale of two is shown. The signal from this scale of two is sent to the cyclotron and controls the oscillator pulse, allowing it to pass or not as is required. It is turned off by the signal from the start of D1 (Fig. 22) and turned on by the signal announcing the end of D2. D2 is also shown in this diagram. It is a conventional univibrator with three ranges controlled by the condensers. The ranges of these three positions run from 50 to 1000 μsec, 1 to 20 msec and 20 msec to 1 sec. This allows a wide range of burst rates. It is initiated by the reset univibrator (Fig. 23) and sends its output to the cyclotron gating scale of two.

FIG. 22

PHASE INVERTER

D_1

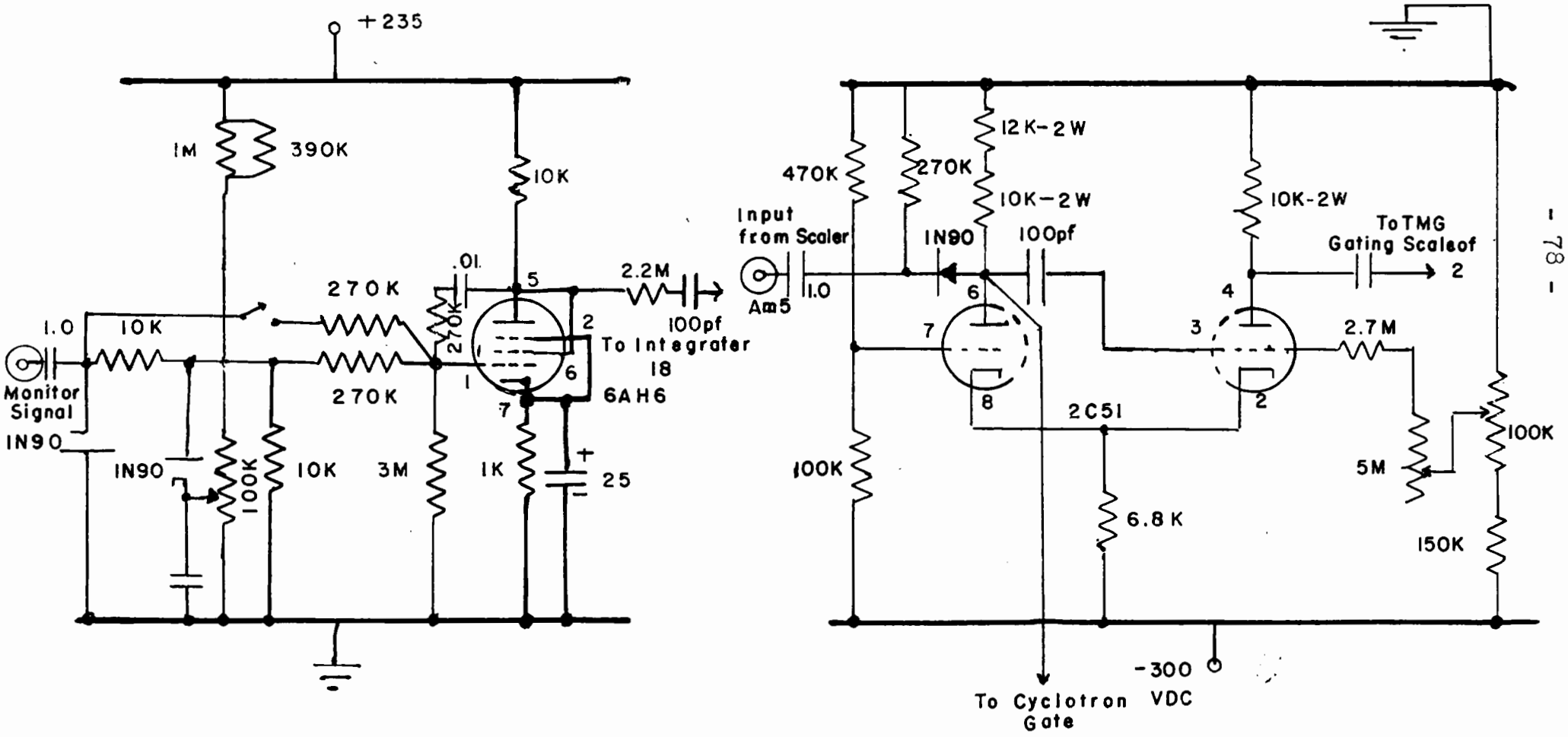

FIG. 23

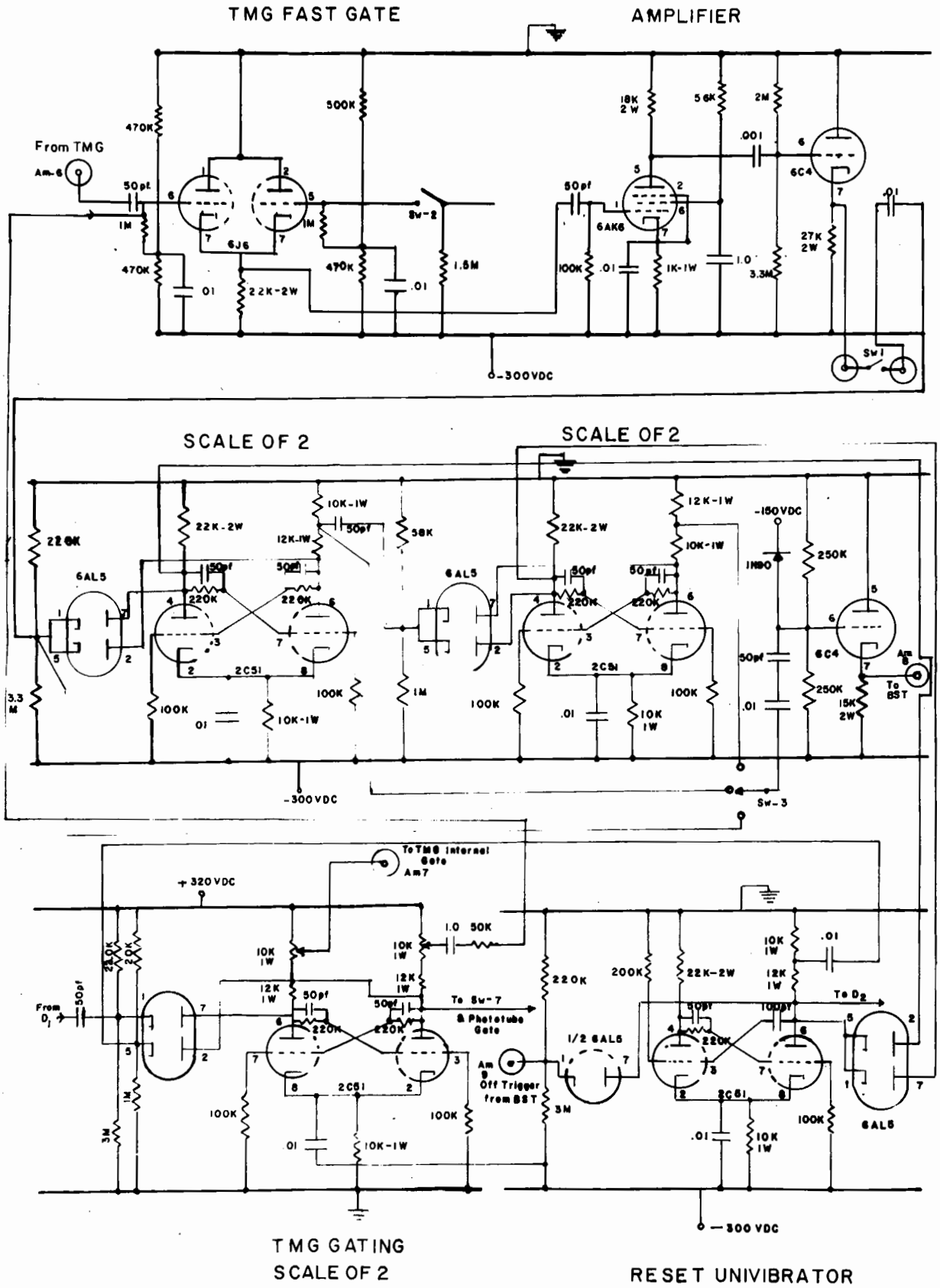
TMG FAST GATE
AMPLIFIER
From TMG
Am-6
470K
500K
50pf
1M
6J6
Sw-2
1.5M
22K-2W
.01
18K 2W
56K
2M
.001
6C4
6AK6
100K
1K-1W
1.0
3.3M
27K 2W
Sw1
-300VDC
SCALE OF 2
SCALE OF 2
6AL5
12K-1W
10K-1W
38K
220K
2C51
100K
10K 1W
-150VDC
1N90
250K
15K 2W
To BST
Sw-3
To TMG Internal Gate Am7
+320VDC
1.0 50K
12K 1W
To Sw-7 & Phototube Gate
From D1
To D2
1/2 6AL5
Am 9 Off Trigger from BST
3M
200K
-300 VDC
TMG GATING SCALE OF 2
RESET UNIVIBRATOR

FIG. 24

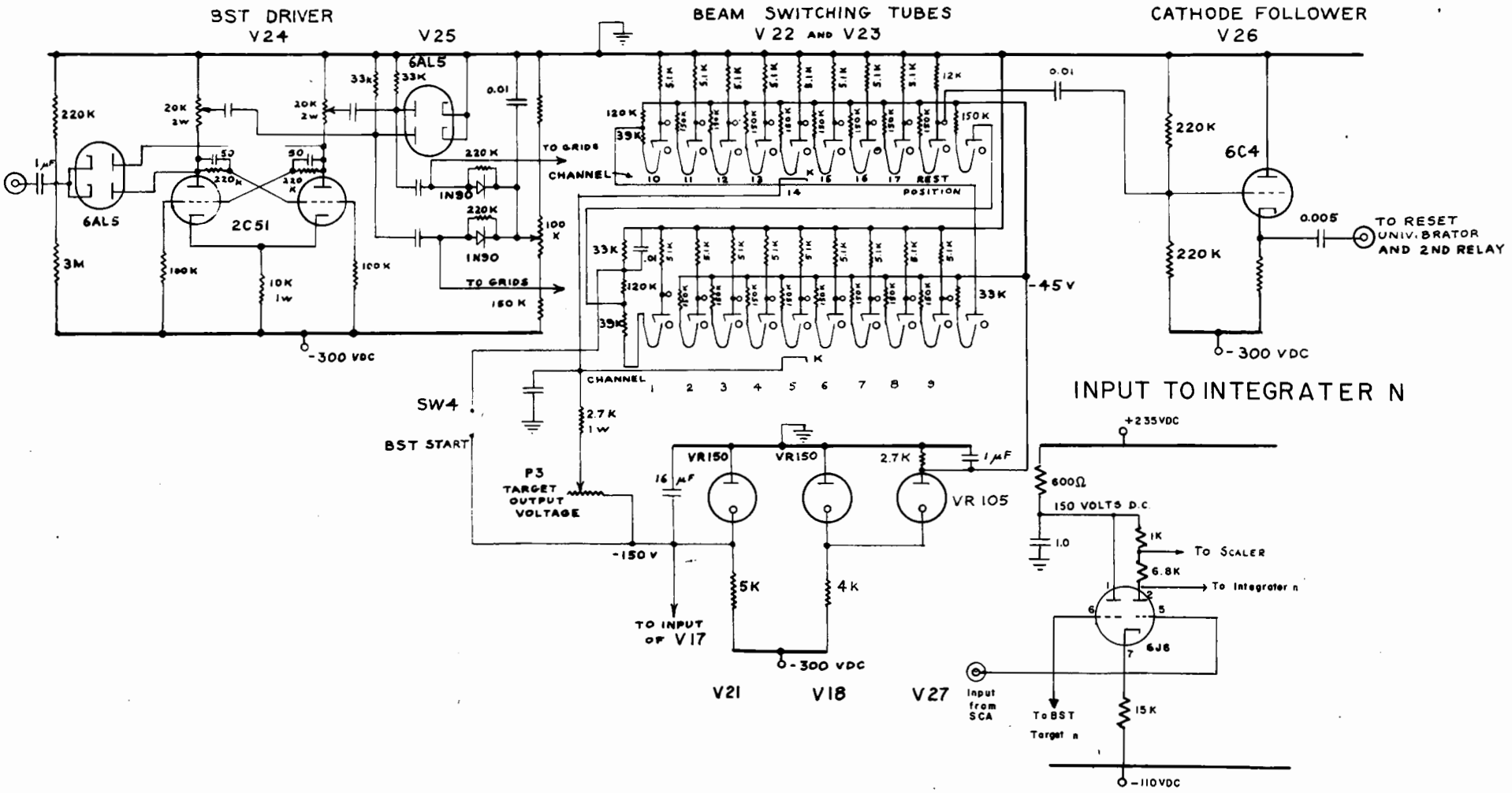
BST DRIVER
V24
V25
BEAM SWITCHING TUBES
V22 AND V23
CATHODE FOLLOWER
V26
6AL5
6AL5
2C51
6C4
220K
20K 2W
33K
0.01
1 μF
3M
100K
10K 1W
100K
IN90
IN90
TO GRIDS
CHANNEL
REST POSITION
120K
39K
12K
150K
-45 V
-300 VDC
0.005
TO RESET UNIV. BRATOR AND 2ND RELAY
SW4
BST START
2.7K 1W
P3 TARGET OUTPUT VOLTAGE
VR150
VR150
VR 105
16 μF
1 μF
-150 V
TO INPUT OF V17
5K
4K
-300 VDC
V21
V18
V27
INPUT TO INTEGRATER N
+235VDC
600Ω
150 VOLTS D.C.
1.0
1K
To Scaler
6.8K
To Integrater n
6J6
Input from SCA
To BST Target n
15K
-110VDC

FIG. 25

P.T. SHORT GATE

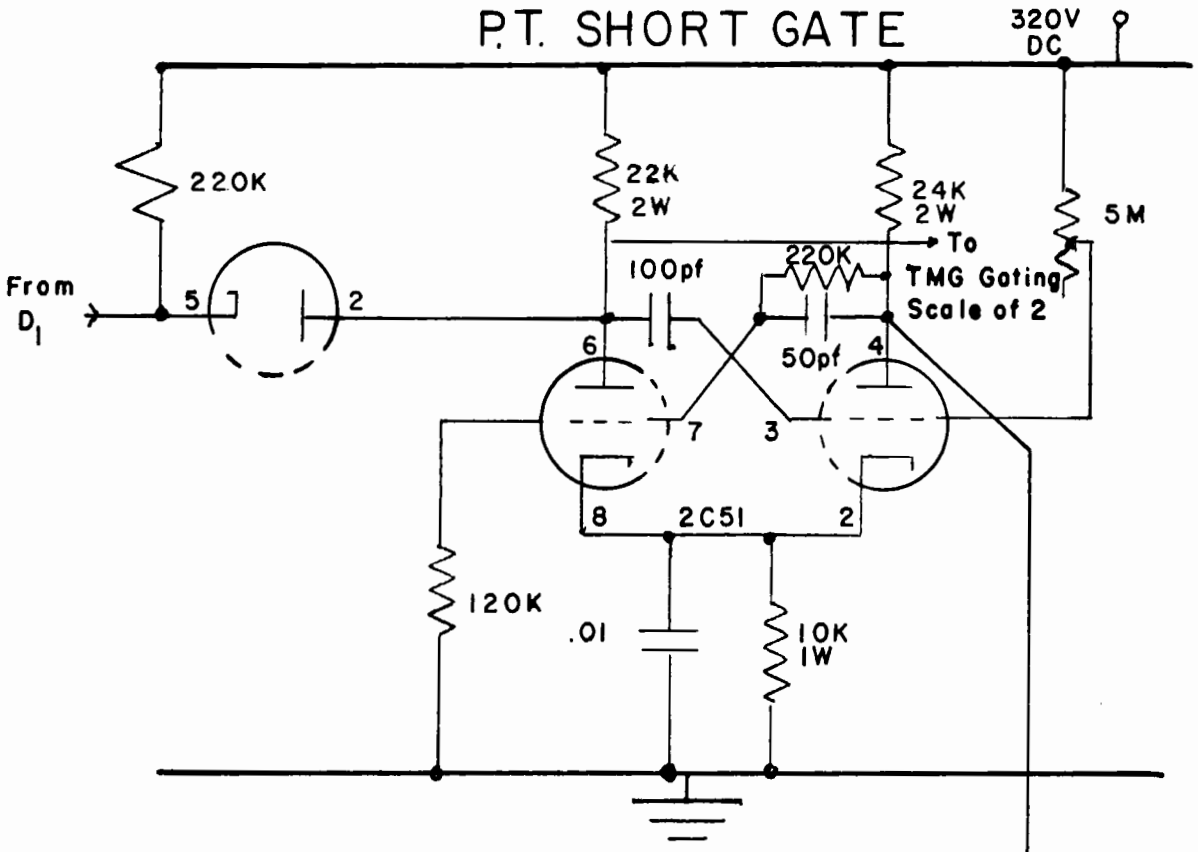

White Cathode Follower

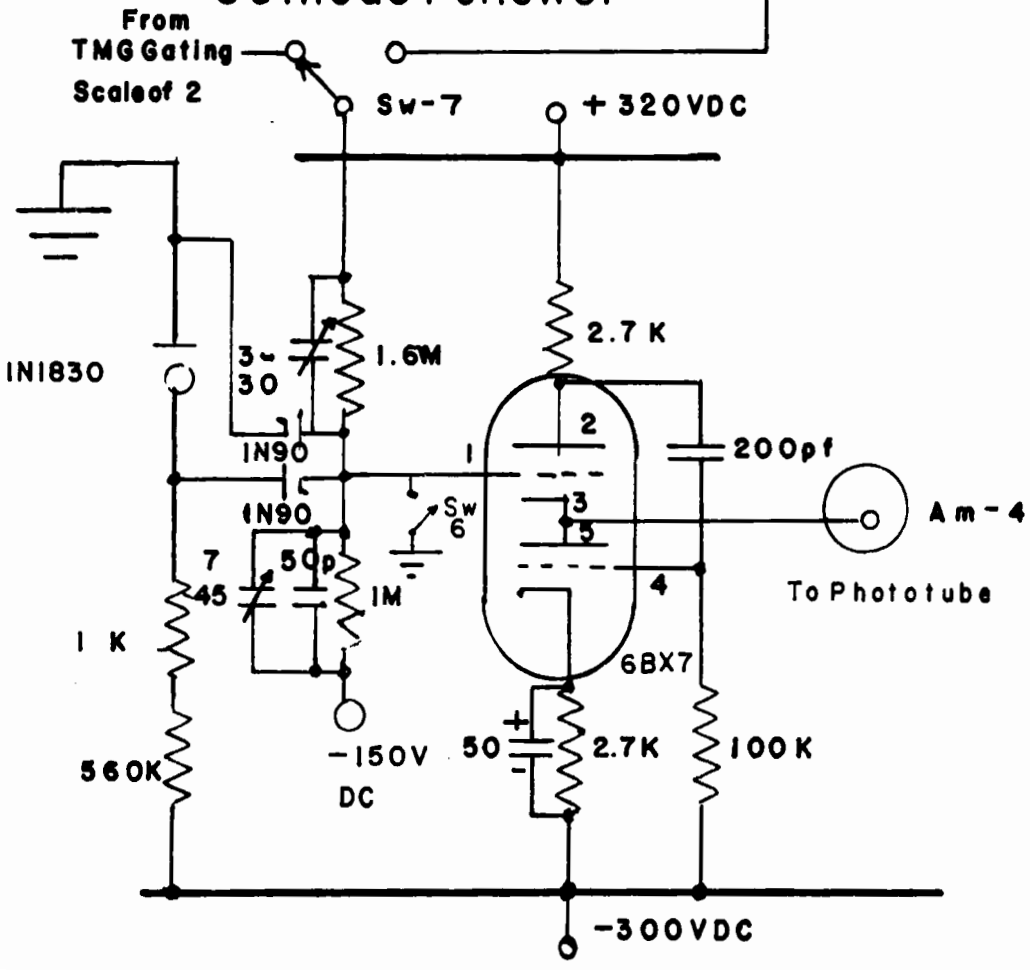

FIG. 26

Cyclotron Gating
Scale of 2

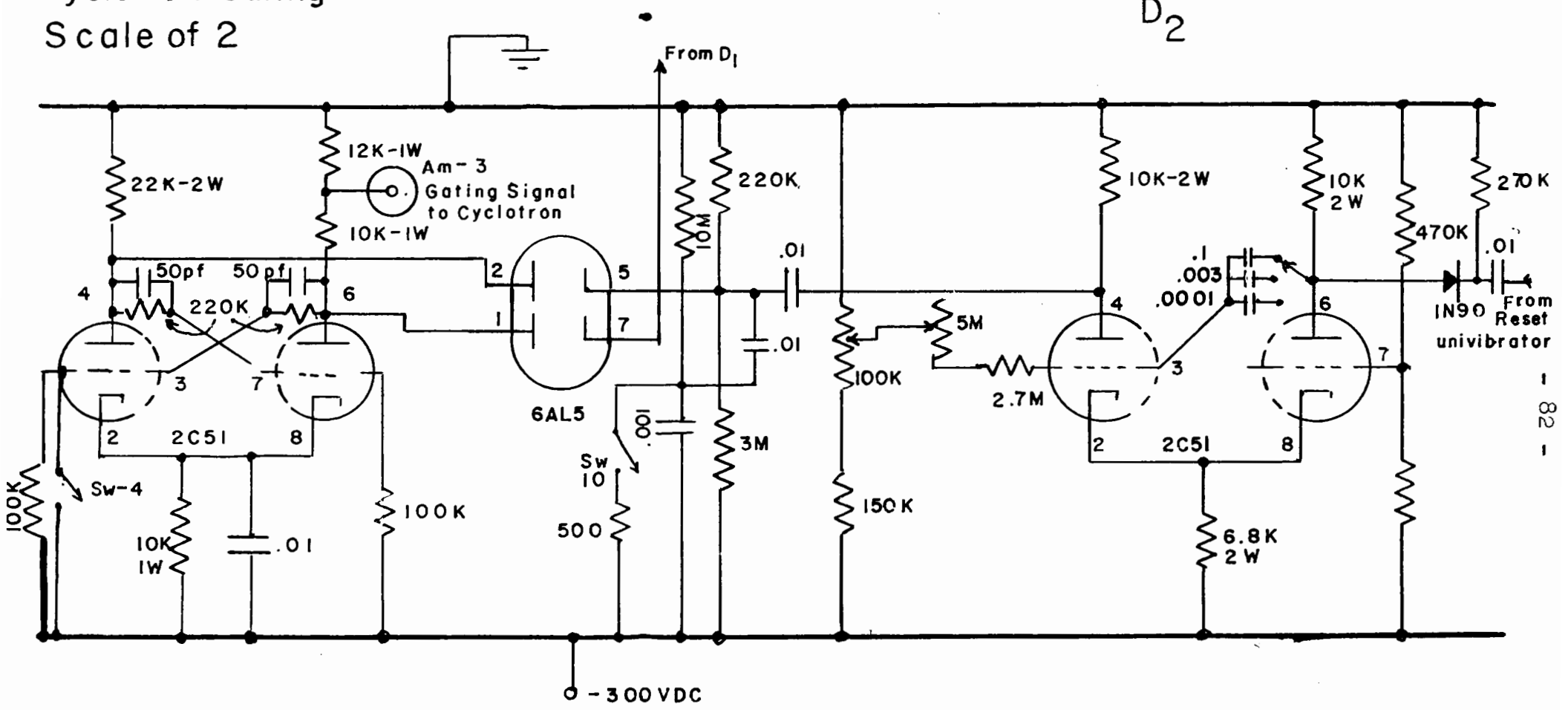

FIG. 27

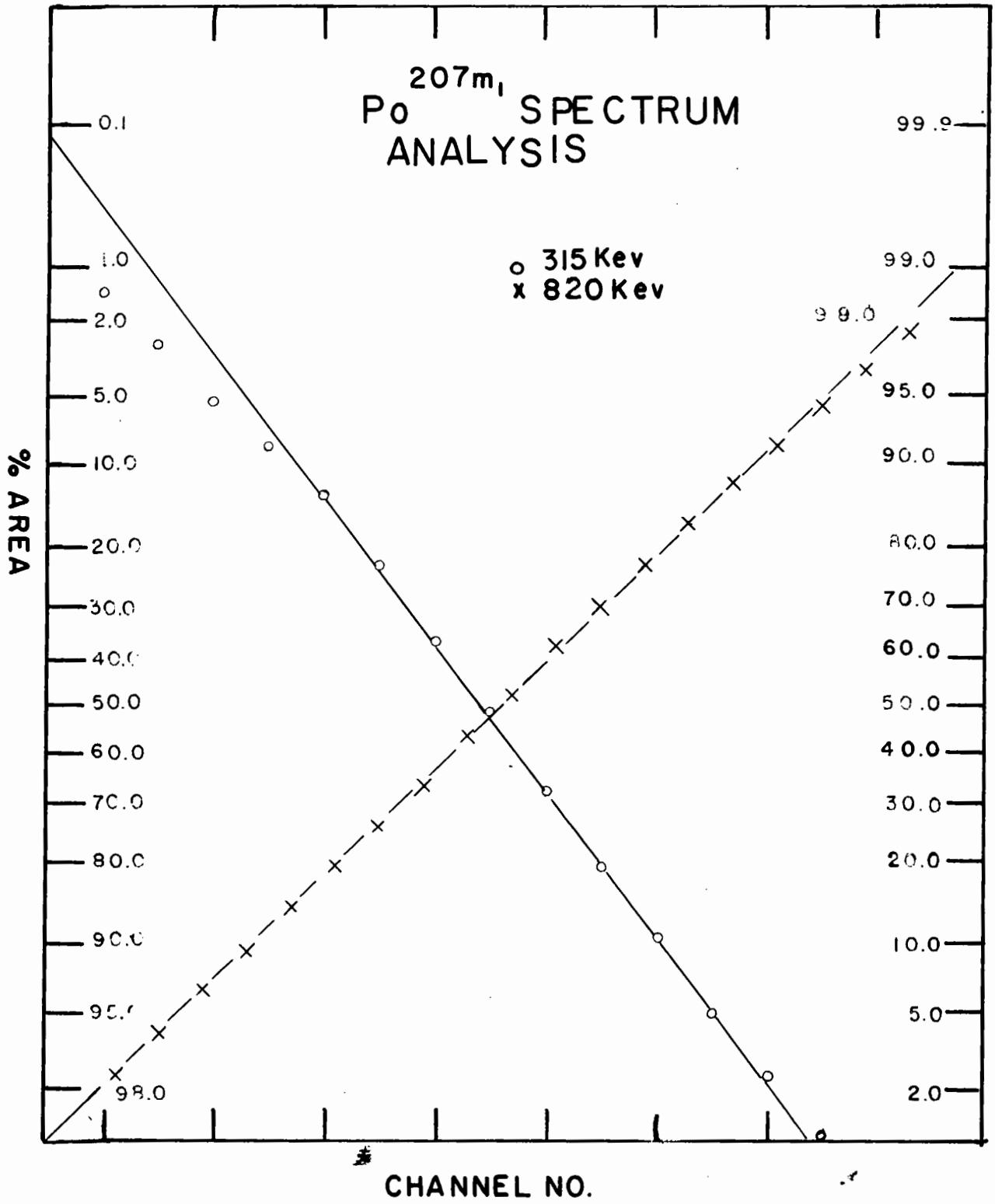
^{207m_1}Po SPECTRUM ANALYSIS
o 315 Kev
x 820 Kev
% AREA
0.1
1.0
2.0
5.0
10.0
20.0
30.0
40.0
50.0
60.0
70.0
80.0
90.0
95.0
98.0
99.9
99.0
99.0
95.0
90.0
80.0
70.0
60.0
50.0
40.0
30.0
20.0
10.0
5.0
2.0
CHANNEL NO.

APPENDIX II

All photo peaks were plotted on probability paper in order to check that they had a normal error shape and hence that they were not really complex and had the correct background subtraction. If either of these effects was present, they were shown as a deviation from a straight line on the probability paper.

A straight line is obtained using this paper if the percent of the total area up to a certain channel is plotted against the channel number. Two examples of this procedure are shown in Fig. 27.

The 820 Kev line of the Po^{207m1} isomer is shown. It is seen that almost every point falls on the straight line and it can be shown that this straight line has a shape that is consistent with the resolution of the crystal. The 315 Kev line is plotted also. This line is seen to deviate rather badly at the upper end. However, most of the points lie on a straight line of the proper slope for the crystal resolution at that energy. Since this peak is superimposed on the Compton of the 820 Kev peak and quite close to the backscatter peak it is assumed that the deviation is due to improper background subtraction. So the points of the straight line were adjusted until they fitted. This was the method used in background subtraction to obtain the proper relative intensities of the peaks. Any deviations from the normal error shape are shown up by this method since a curve will not fit a straight line.

This method was used when the 280 Kev peak was found to be

double. The plot could not be fitted to a straight line.

Therefore the method is useful in analyzing complex spectra. This method was suggested by W. White of the Radiation Laboratory and has since been published by I. Boekelheide (36).